12-2006

Application of Energy Analysis to the Problem of Propulsion Driven Nutation Instability of Spin Stabilized Spacecraft

Tina Morina Rice
University of Tennessee - Knoxville

To the Graduate Council:

I am submitting herewith a thesis written by Tina Morina Rice entitled "Application of Energy Analysis to the Problem of Propulsion Driven Nutation Instability of Spin Stabilized Spacecraft." I have examined the final electronic copy of this thesis for form and content and recommend that it be accepted in partial fulfillment of the requirements for the degree of Master of Science, with a major in Aerospace Engineering.

Gary A. Flandro, Major Professor

We have read this thesis and recommend its acceptance:

Kenneth R. Kimble, Uwe Peter Solies

Accepted for the Council:
Carolyn R. Hodges

Vice Provost and Dean of the Graduate School

(Original signatures are on file with official student records.)

To the Graduate Council:

I am submitting herewith a thesis written by Tina Morina Rice entitled "Application of Energy Analysis to the Problem of Propulsion Driven Nutation Instability of Spin Stabilized Spacecraft." I have examined the final electronic copy of this thesis for form and content and recommend that it be accepted in partial fulfillment of the requirements for the degree of Master of Science, with a major in Aerospace Engineering.

Gary A. Flandro
Major Professor

We have read this thesis
and recommend its acceptance:

Kenneth R. Kimble

Uwe Peter Solies

Accepted for the council:

Anne Mayhew
Vice Chancellor and
Dean of Graduate Studies

(Original signatures are on file with official student records.)

Application of Energy Analysis to the Problem of Propulsion Driven Nutation Instability of Spin Stabilized Spacecraft

A Thesis
Presented for the
Master of Science
Degree
The University of Tennessee, Knoxville

Tina Morina Rice
December 2006

DEDICATION

This thesis is dedicated to my family for all of their love and support throughout my education, especially my mother and father, Morina and Shelia Joe Rice, and my aunt Lorraine Compton. When I had troubles and was in doubt, they all believed in me and told me I could succeed.

ACKNOWLEDGEMENTS

I would like to express my sincere gratitude to all members of my thesis committee: Dr. Gary A. Flandro, Dr. U. P. Solies, and Dr, Kenneth Kimble. I would also like to extend thanks to fellow students for their assistance and much appreciated support when needed: Richard Lewis, Paul Gloyer, Esam Abu-Irshaid, Daniel Lehman, Gail Wells, Ifeyinwa Oranugo, and Catherine Kelly.

ABSTRACT

Propulsion driven nutation instability in spin stabilized spacecraft was first observed in the late nineteen seventies. It's often referred to as the *PAM-D coning anomaly,* as it first occurred in the McDonnell Douglas Payload Assist Module (PAM-D). Propulsion driven nutation instability is a performance degrading phenomenon that occurs in spin-stabilized spacecraft used for the raising of satellite payloads to geosynchronous orbit. It is characterized by a coning (wobbling) motion that grows to a large degree during the final seconds of motor burn. The instability is clearly related to the increased size of the rocket needed to support the increasing payloads to be taken into orbit. This nutation wastes motor impulse and overtaxes the attitude control system after burn. The remedy to date has been the use of a strap-on attitude control device.

Several mechanisms have been proposed and eliminated due to lack of correlation with observed nutation features. The mechanisms of slag sloshing and jet gain both showed similarities to the observed disturbances. Jet gain shows the most promise in understanding the nutation phenomenon. Neither mechanism has yielded suitable conclusions to establish proper nutation prevention criteria for future designs.

Through analysis of the effects of energy loss due to mass transfer on the spacecraft's kinetic energy balance, it is shown that nutation can be seen to develop without the need for in depth analyses.

TABLE OF CONTENTS

Page

LIST OF FIGURES

Page

LIST OF ABBREVIATIONS

PAM-D	Payload Assist Module
deg	degrees
ft	foot or feet
s	second
hr	hour
in	inch or inches
lb	pound (force)

LIST OF SYMBOLS

D	Diameter of Chamber
I	Pitch/Yaw Moment of Inertia
I_3	Transverse Moment of Inertia
L	Length to C.G.
mdot	Mass Flow Rate
R	Radius of the Chamber
v_b	Burn Velocity of Propellant

Greek Symbols:

ε	Rossy Number
λ	Nutation Frequency
ρ	mean density of gas in the chamber
σ	Inertia Ratio: I_3 to I
τ	Time Constant for divergence
ϖ	Transverse Angular Velocity
Ω	Spin Rate about Roll Axis

CHAPTER 1

INTRODUCTION

Background - Problem Statement

The use of spin stabilized systems for orbit-raising of payloads was first employed in the late sixties. Spin stabilized systems offer an advantage to non-spinning systems by minimizing the effects of mechanical energy dissipation such as tumbling of prolate spacecraft bodies, bodies that have a longer axial length than radial length. Spin stabilization is a simpler attitude control alternative to three axis control systems; it makes use of natural gyroscopic resistance to external disturbances to remain stabilized about the transverse axis. (1)

Each system is comprised of three major parts: a solid propellant rocket motor, a payload attachment structure, and a spin table/separation module. During orbit-raising, the spacecraft is released from a carrier with some spin induced angular rate and the motor is ignited upon separation distance.

When spin is employed to stabilize a satellite, it is assumed that there will be no lateral angular velocity components due to gyroscopic effects. However, upon motor ignition, a slight tip-off induced lateral wobble remains from release. Previous theories of jet damping, to be discussed later, predicted that the wobble would be eradicated shortly after ignition. However, upon reaching mid-burn, the small lateral oscillations begin to grow instead of decay. At motor burnout, the final angle of nutation can be as much as twenty degrees.

Figure 1 – Internal View of a PAM-D Motor

This disturbance did not occur until the size of payloads began to increase. The need to deliver greater impulse required the employment of a larger solid rocket motor. A scaled up version of the smaller Star 37 motor was employed known as the Star 48 shown above in figure 1.

The central concern is that there is a resulting degradation of performance that is undesirable. The vehicle experiences a dissipation of delivered motor impulses as the nutation grows. This is undesirable effect since every gain in impulse is a difficult and costly effort not to be wasted. And, as payload mass increases, there is a greater impulse

requirement to ensure mission success. Some space flights have failed to perform their designated mission as a result of nutation.

To date use has been made of strap-on attitude control systems in an attempt to lend some control to the nutation by providing impulses to correct for significant angular deviations. These control devices cannot always correct for the oscillations as the nutation behavior cannot be accurately predicted for proper application of corrective impulses. The use of spin stabilization is supposed to eliminate the need for a control system, and the use of such a system only adds unneeded weight, complexity, and cost to the vehicle. If the cause of this problem can be found and a true solution provided, there will be no further need for these attempts at temporary fixes. (2)

Data taken from twenty flight vehicles has shown that certain properties related to geometry, mass, and burn time have a direct effect on the disturbance growth. However, a greater physical understanding of what is actually occurring within the system is needed to find a solution. There have been as many as twenty proposals as to the origin of the disturbing mechanism; many have been dismissed due to a lack of agreement with certain features of the nutation phenomenon present in all data.

The two most widely supported theories that show correlation with data fail to bring about a final solution for prevention of the nutation phenomenon. These two mechanisms require a complex analysis of the system dynamics and reactions within the gas flow. Instead of going into such an in depth system analysis, a more simple evaluation of the kinetic energy of the system is presented. This analysis will show that growth of the nutation angle throughout burn can be predicted. Figure 2 shows a rendition of the nutation growth as it occurs.

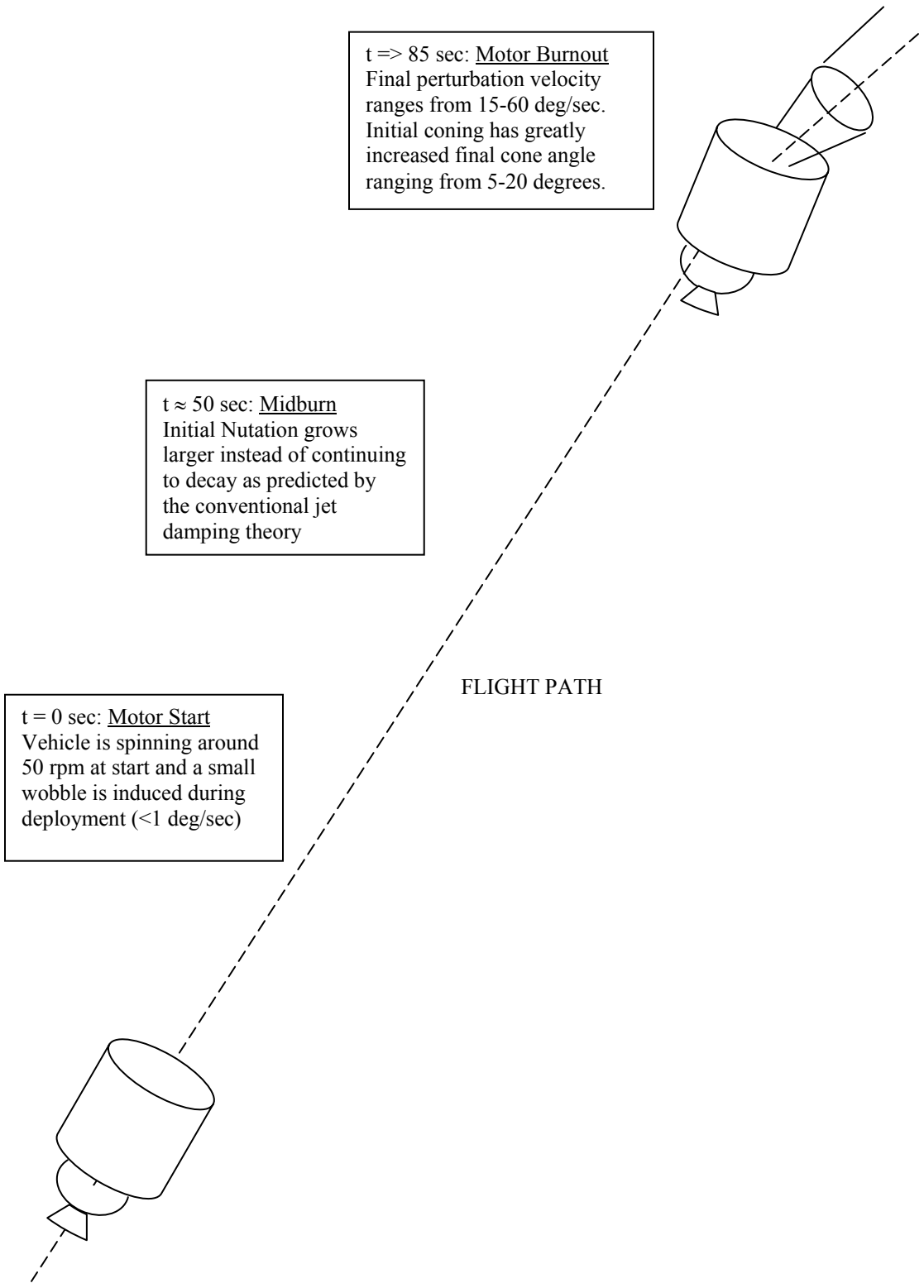

Figure 2 –Nutation Growth during Motor Burn

Body Fixed Coordinate System of Satellite

To understand the angular notation expressed throughout this study, an introduction to Euler angles is necessary. Through application of this notation, the spacecraft dynamic motion can be understood. The specific Euler rotation sequence used is commonly referred to as the aerospace sequence, most recognizable from aircraft applications. For each rotation of a vehicle in space, the axes are continuously reassigned with the body throughout angular motions as they are body-fixed. This discussion does not delve into the mathematics of sequences. For a complete understanding of rotations and their sequence multiplications refer to Spacecraft Attitude Dynamics and Control by Thomson.

Figure 3 correspond to the body-fixed coordinate system used. The axis about which spin occurs is commonly referred to as the roll axis also known as the axial or longitudinal axis. The yaw and pitch axes, are those about which motion is supposed to be minimal during spin-up. The labeling and positioning of the axes relative to each other can be seen in figure 3. Since the body is symmetric about the longitudinal axis, the yaw and pitch moments of inertia are equivalent and are herein referred to as the lateral moment of inertia.

The common rotation sequence about the body-fixed axes corresponds to varying rotations about the respective pitch, yaw, and roll axis. Figure 4 shows such a sequence and the corresponding angles of rotation. (3)

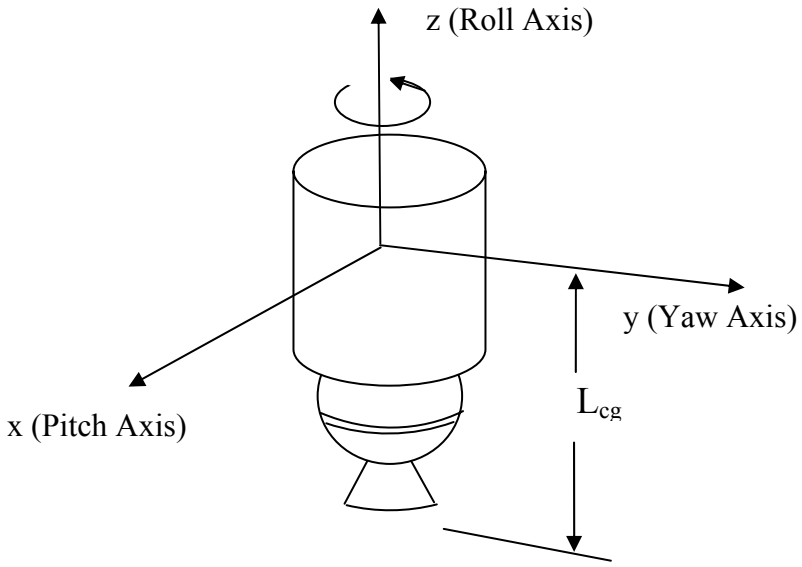

Figure 3 – Spacecraft Body-Fixed Coordinate System

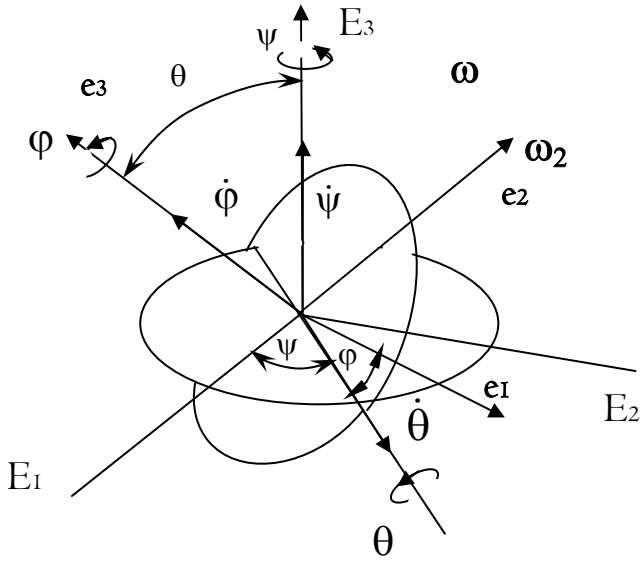

Figure 4 – Typical Aerospace Rotation Sequence

Precession and Nutation

This sequence of rotations is employed to represent the torque free motion for a body with rotational symmetry. Figure 5 aids in visualizing this motion. Placing the body within an inertial reference frame, the angular momentum vector **h** is placed along the E_3 axis. Precession is the naturally occurring gyrodynamic motion of the systems angular velocity vector about this angular momentum vector. Spin is induced about the e_3 axis of the body-fixed system. Through gyroscopic motion of the body, the accumulating angular momentum vector imparts a nutation about the e_1 axis. (1) A constant angular momentum rate vector is considered to be fixed in space; the nutation angle remains constant as well. It will be shown that for a variable mass system that with changing angular momentum, the nutation angle changes as well. Figure 6 shows a representation of this coning motion.

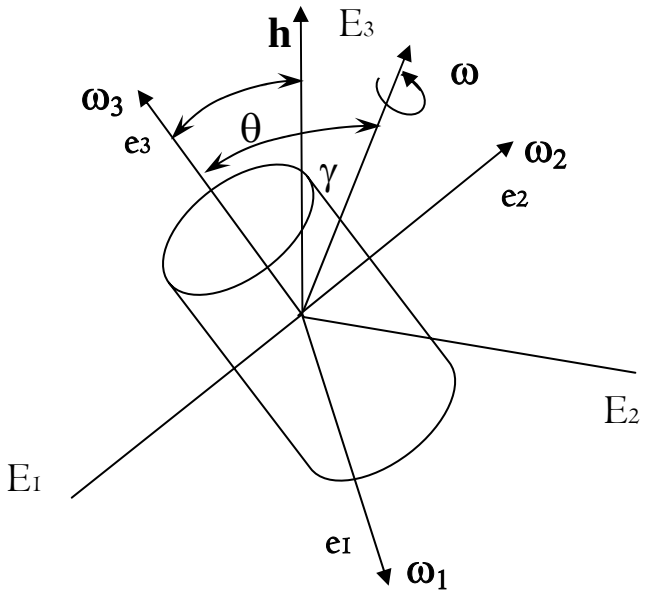

Figure 5 – Symmetric Body Experiencing Torque Free Motion

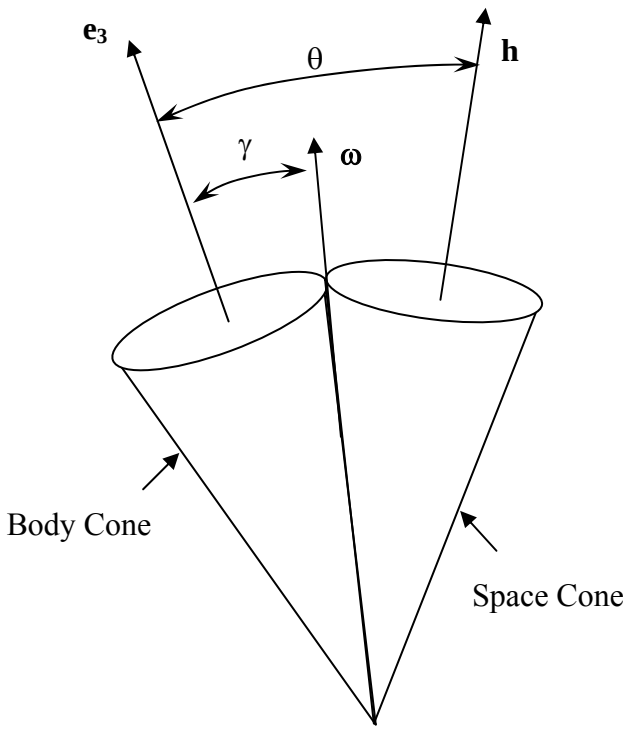

Figure 6 – Direct Precession of a Prolate Body

To put precession and nutation in a common perspective, one can visualize the motion of the earth's spin axis. The earth's axis spins and throughout this spin, the axis precesses in a long 26,000 year cycle. This angle of precession, commonly referred to as tilt of the earth's axis, is roughly 23.5 degrees. The axis also experiences nutation at a small magnitude of about 20 arc seconds. In the case of the earth, this nutation is due to the gravitational tug of war between the sun and the moon. The period of nutation is on the scale of 18 years, mainly influenced by the precession of the moon's orbital nodes. Figure 7, obtained from the online encyclopedia, Wikipedia, is provided to help visualize this motion. (4)

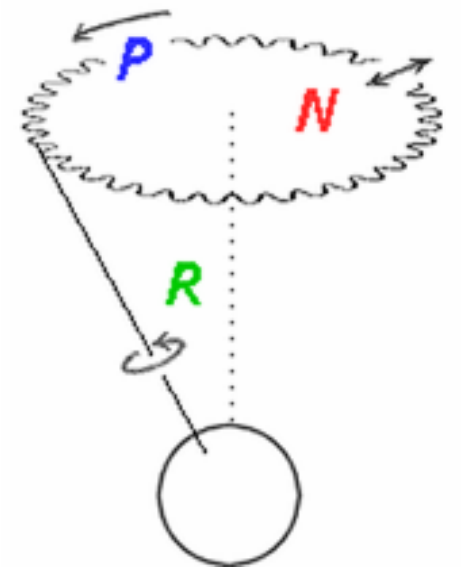

Figure 7 – Precession and Nutation of the Earth's Axis

Objectives

The purpose of this study is to inform the reader of the occurrence of nutation instability and present previous work that has been done in attempt to understand the phenomenon. Through formulation of kinetic energy for varying mass flow, it will be shown that nutation growth occurs in certain spin stabilized vehicles.

CHAPTER 2

Proposed Mechanisms

As stated in the introduction, as many as twenty mechanisms have been previously suggested as to the origin of nutation instability. Through examining recorded data from rate gyroscopes and accelerometers, it seemed apparent that there is a dynamical interaction with the solid rocket motor burn. (5) Through careful evaluation and due to a lack of agreement with certain key features of the nutation phenomena all but two mechanisms were dismissed. The choices were narrowed down to the slag sloshing model and the jet gain or gas dynamic coning effect. Both have their supporters and both represent very different mechanisms

Telemetry Data

Before going further in an analysis of the problem, it is important to present data that has been observed and recorded from flights and experiments. Very little data has been acquired to help analyze the coning problem. Although some has been recreated experimentally, there has not been any extensive experimental testing; only a large range of data acquired in actual flights has been collected. Since there is not enough data available to solve the problem empirically, there must be a greater understanding of the actual disturbance mechanism. To understand this mechanism, the rate gyroscope and accelerometer data taken from the twenty flight vehicles was compared and analyzed.

Through this comparison of data, general features of a disturbing mechanism were determined.

The most useful data comes from the rate gyroscope. The pitch and yaw angular rate are shown to oscillate from motor ignition until burnout. For the first half of the motor run, the initial release-induced oscillations of about one degree/second appear to be damped. It is presumed that the classical jet damping effect is in action. All data sets taken show this apparent damping until mid-burn. The oscillations then begin to increase exponentially until the end of motor burn when they cease. It is believed that perhaps this growth occurs because the jet damping effect is not as large as predicted from theory. The jet damping is also shown to rapidly decrease instead of increasing as predicted as the burn progresses due to the center of mass moving forward and the combustion chamber length increasing. The initial induced wobble is kept to a constant magnitude, but as the rockets moment of inertia decreases due to propellant consumption, the vehicle becomes more susceptible to disturbance. Also, the angular velocity perturbations move in a retrograde motion opposite to the axial spin; the yaw signal leads the pitch signal by almost exactly 90^{O}. This eliminates any such mechanisms as thrust misalignments, non-uniform propellant burn, and center of mass offsets, as they cannot generate such motion.

From analysis of the data, it is clear that there are certain general features to the nutation instability that occur in all flight data. It has been determined that these features must be represented in whichever model of a disturbing mechanism is chosen. The coning clearly originates form inside of the rocket motor with instability growth ceasing upon motor burnout. It appears that there are resonant characteristics as shown in recorded frequency and nutation growth graphs. The system must be a self-excited

system in which the disturbing torque and nutation angular velocity are proportional in some way. (2)

Now that the reader has knowledge of the observed behavior, the current disturbing mechanisms still under study will be presented. The gas dynamic mechanism will be shown to be the more likely mechanism in action. The flow set forth in the jet gain mechanism is assumed to be present when performing the energy analysis although the analysis does not focus on the internal flow interactions presented in the model. Following the introduction of both mechanisms, these flow patterns will be discussed in the system description. Figure 8 shows a comparison of the chamber effects exhibited in both models.

Slag Sloshing Mechanism

In the slag sloshing mechanism, as seen in the top corner of figure 8, it is assumed that aluminum oxide slag is produced during combustion. It then accumulates in the aft closure of the chamber during motor burn gathering in a pool that sloshes in response to any wobbling of the spacecraft.

Many investigators prefer this as the more likely disturbing mechanism because similar nutation behavior has been observed in other space vehicles due to liquid fuel stores. It is considered that such a build up could be possible under strong exertion of gravity due to axial acceleration and centrifugal forces. The relative motion of this sloshing slag creates an offset in the center of mass which results in a thrust induced torque. The system can become unstable to small disturbances if the offset is in phase with the angular velocity vector relative to lateral motion. (6, 7)

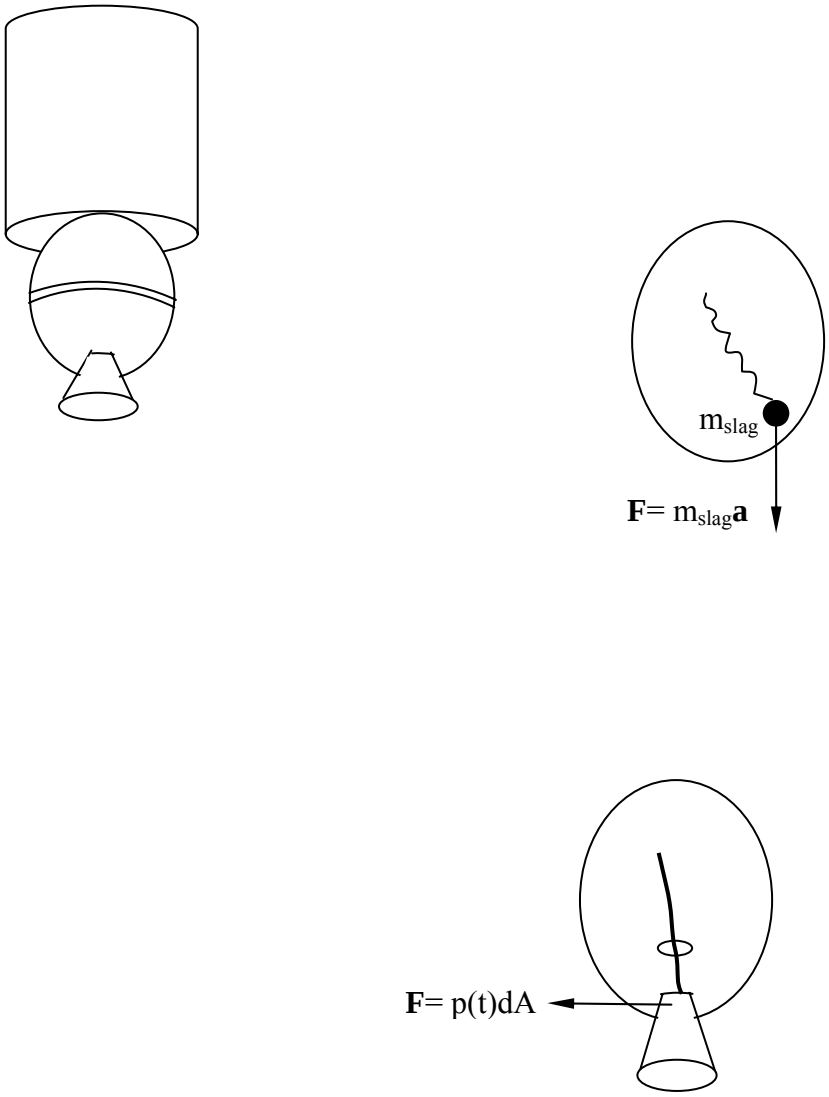

Figure 8 - Slag Sloshing Model and Jet Gain Effects on Chamber

In order to produce the observed nutation behavior, the system has to be modeled through use of dynamic analogues such as spring damper systems and pendulums. Through 'toning' the system with application of unknown parameters the phenomena and observed data can be reproduced for the early burn stage. Adding parameters that are not there in order to produce desired behavior is a method often employed by dynamicists; this is why they are often supporters of the slag-sloshing theory. However, this leads to what others view as the many shortcomings of the slag-sloshing theory.

The nutation growth follows an exponential trend, and the slag theory can initially reproduce the early burn growth. However, due to its nonlinear modeling it quickly tends to saturation or a limit cycle type behavior as the nonlinear effects take over. An assumption of a high slag accumulation rate can avoid this limiting, but there is no supporting reason for this to be realistic. Such an accumulation leads to a behavior suggestive of a reciprocating transfer of energy and momentum between the slag and the vehicle, and this is not in agreement with linear predictions.

From this point on, the assumption of a high accumulation rate must be maintained. However, linear fluid slag models run with this assumption have shown that the slag does not behave like the dynamic analogues used for the initial formulations.

Several other weak points exist in this theory. This slag behavior cannot be measured directly during burn. It must be deduced from solidified fragments remaining in the motor case after testing. There has also been much difficulty in properly 'toning' the change of mass center to be in phase with the observed driving moment. Possibly the greatest hindrance to the model is the lack of complete understanding of the slag accumulation itself and the presence of possible effects such as mixing. All of these

doubts set forth in a proper presentation of slag sloshing theory essentially eliminate it. Thus the related flows and behavior do not require further attention in the illustration of a solution to the problem of nutation instability. (6)

Gas Dynamic (Jet Gain) Mechanism

The gas dynamic driving mechanism associates the nutation disturbing mechanism with the interactions between the wobbling motion of the vehicle and the internal gas flow of the motor. It also incorporates a type of sloshing motion in response to the motion of the vehicle, but it is a movement of the internal gas flow. The mechanism is closely related to and incorporates the classic jet damping effect; this is where the name jet gain comes from. During burn, the jet damping seems to damp out any wobble initially; but as the burn proceeds, data shows that a force with the same apparent magnitude as the jet damping seems to begin acting as a driving force. Figure 9 shows a comparison of the classically predicted and observed behavior.

This force is believed to develop from a combination of internal gas flow characteristics discussed in detail in the system discussion. The initial wobble imparted to the vehicle induces a traveling wave within the internal gas medium. This motion has an unsymmetrical pressure distribution effect on the internal walls of the chamber. An asymmetrical flow field is developed exerting a sideways deviation in the exhaust flow. This in turn exerts the unbalanced side force that applies the disturbing torque. The torque becomes a destabilizing effect results when these traveling waves are in resonance with the vehicle precession frequency.

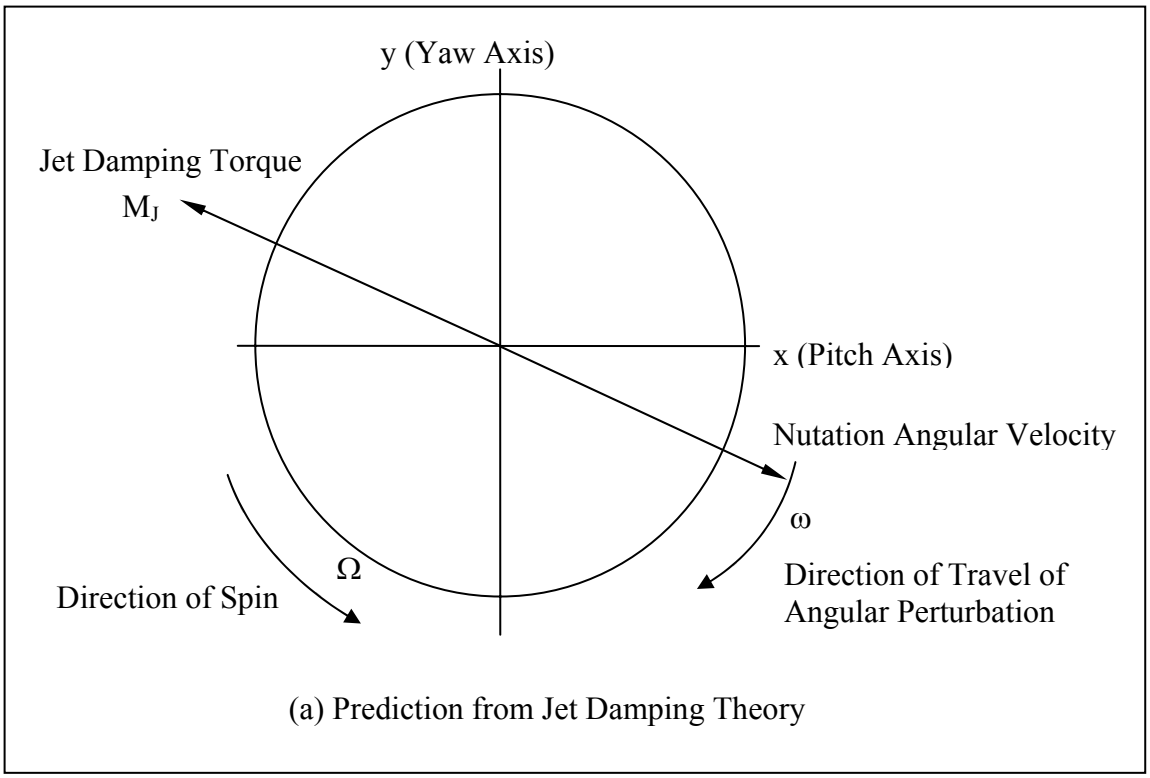

(a) Prediction from Jet Damping Theory

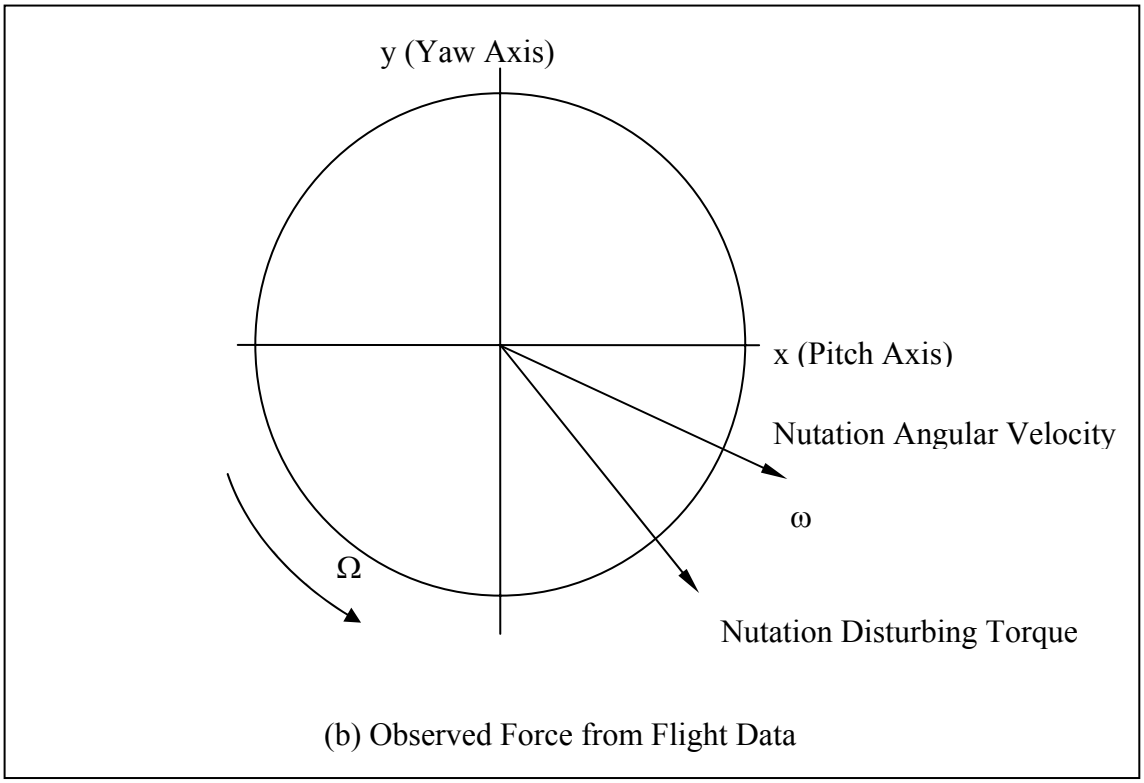

(b) Observed Force from Flight Data

Figure 9 - Comparison of Classically Predicted and Observed Interaction Moments

Through Air Force sponsored studies of cold flow simulations, a solution for the destabilizing torque was developed that showed close agreement qualitatively with experimental data. A computer algorithm developed from these experiments closely correlated with telemetry data from some of the PAM-D spacecraft. The results were also able to be applied to the smaller Star 37 motor. There was no need to apply unknown parameters to make the solution agree with data. The only drawback is the extreme difficulty of a quantitative mathematical formulation due to the complexity of the gas dynamics within the flow. In the following section, the flow ideals and their effects on the driving mechanism will be set forth but mathematical details will not be presented. As the legitimacy of this model is not in question, the in depth derivations would only serve to distract from the subject. (6)

CHAPTER 3

System Discussion

What is Jet Damping?

Jet damping is the response of the flowing combustion gases to any angular motion of the rocket motor about an axis normal to the axis of symmetry. It is not related to frictional damping; it is simply the reactive force of the gases to the lateral perturbations exerted by the chamber walls.

The Origins of Jet Damping

Jet Damping was first noticed many years ago in unguided ballistic rockets. The initial oscillations resulting from release were seen to damp more quickly than expected from external aerodynamic forces alone. It was determined that the internal gas flow was responding to the angular motion of the vehicle to produce this damping effect. It seemed reasonable to assume the internal gas flow followed straight streamlines having the same effect as the external flow had on the lateral motion. In effect, the internal flow remains uniform as the chamber walls change angle with respect to the flow producing aerodynamic restoring forces inside the chamber which is the jet damping effect.

Since there is a net torque opposing the angular motion, an asymmetrical pressure pattern must be in action. Assuming the flow moves uniform and parallel to the motor axis, then as the chamber moves laterally, this pressure pattern acts as a net force applied to the gas stream. This force arises from integrating the pressure forces at the interface

between the gas stream and the chamber walls. The gas flow reacts to the forced change of direction by applying a force to the wall to oppose it. (6)

Shortcomings of Jet Damping

This assumption that the gas flow is along straight streamlines may be sufficient for analyzing small nonrotating rockets with short burn times. However, for large spinning space motors with longer burn times, such a simple model must be reconsidered.

In the classic model, it is assumed that the gas is a continuous medium. It behaves like a rigid body when acted upon by an outside force, thus applying an opposing force in kind. However, the gas is not truly rigid, it is deformable. Therefore, if a gas particle is acted upon by an outside force, instead of maintaining a constant path, its velocity and path will change. The previous model worked for smaller rockets since the particles moved quickly enough through the system that the streamlines were not affected. For larger spinning rockets, the longer residence time of the gas particles within the system allows more exchange of angular momentum having an altering effect on the gases reactive forces. The flow streamlines become significantly curved and there is an appreciable radial component of velocity. This is due to the effect of Coriolis forces.

In the case of spinning rockets, the inertial Coriolis force is the main contributor of the jet damping phenomenon. When the force acts on a gas particle, it acts perpendicular to both the system angular velocity vector and the local velocity vector of the particle. A particle on the opposite side of the chamber experiences the same Coriolis force thus contributing an asymmetrical force. This is the reactive force of the gas tending to resist the angular motion in jet damping. (7)

For a complete understanding of the internal flow within the chamber, it is necessary to go beyond the simple flow suggested in the jet damping model. The composite flow field present within a spinning, nutating rocket consists of the superposition of three components of flow: the mean flow, vortex flow, and the time-dependent part of the flow. Once the composite flow is developed, the origin of the driving effects in the gain model is more evident.

Mean Flow

The mean flow is the flow assumed to be steady and symmetrical as in the classical jet damping calculation. It can also be uniform, one dimensional axial flow. This assumption that the Coriolis force produced from the chamber rotation is balanced by an unsymmetrical pressure distribution is appropriate if no other gas motion is considered. However, this is not a realistic flow scenario; other flow components need to be added to the flow model. Figure 10 shows the three components of flow considered to be present in the chamber. (7)

Vortex Flow

Visualizing the flow induced from the motion of individual gas particles, the next flow component is presented. A coordinate system rotating with the chamber boundaries can be used to envision the motion of gas particles emerging from the burning surface. As the propellant surface burns, the emerging gas particles carry a spin induced circumferential momentum component that must be considered.

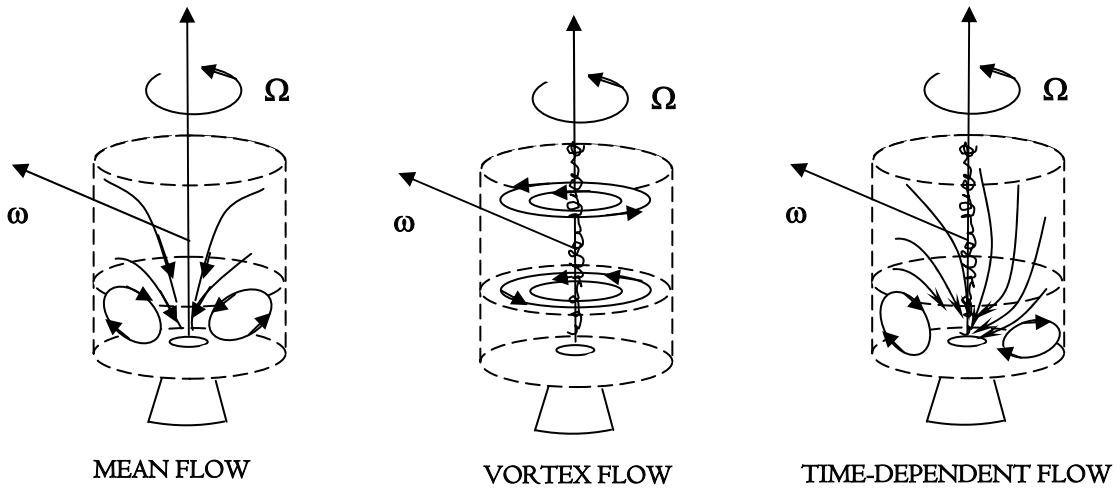

Figure 10 – Three Components of Flow

If the vehicle is in spin about its axis of symmetry, then the flow passes axially out of the nozzle. As the flow approaches the nozzle, the gas particles are forced towards the chamber axis. The speed of the particles must increase in order to maintain momentum. A strong swirling effect known as a Rankine vortex is developed within the chamber. It is not a simple turning "wheel" motion. A familiar example that one can relate to is a tornado; the increased speed at the bottom lends to its destructive nature. As the surfaces burns back the vortex speed increases to maintain angular momentum.

These vortices combine to affect vehicle spin rate during motor burn. Assuming that the spin rate increases due to roll moment of inertia decrease as propellant is consumed doesn't seem to account for the change in spin rate. This can be shown through a simple momentum balance. The radial path distance traveled by the gas particles as the propellant burns increases throughout motor burn just as roll moment of inertia decreases thus contributing to increased axial spin growth. The presence of this

effect has been detected in PAM-D data as an increase in the spin rate throughout motor burn. This vortex flow combines with the simple mean flow to form a more complete model of the mean flow through the chamber. (7)

Time Dependant Flow

In figure 9 above, the jet damping force is balanced by an oppositely acting force. The lateral perturbation angular velocity vector of the gas particles acts relative to the chamber opposite the direction of vehicle spin. This creates a time-varying force that in turn imparts a rising and falling effect on the lateral gas motion within the chamber. This represents a lateral angular momentum that travels in a loop about the interior of the chamber. Conservation of momentum principles apply to the lateral angular momentum just as they do to the axial angular momentum. Particularly as the flow moves radially inward and rearward toward the nozzle, conservation again insists that the lateral angular momentum increases as it does axially.

This motion of gas within the chamber is believed to be the major contributor to the recurrence of increased nutation oscillation in the jet gain model. It is considered similar to that of inertial waves. This circulating motion occurring in spinning gas creates a wave-like motion that is time-dependent. Analysis of the governing equations shows them to be hyperbolic in a certain frequency range. This range happens to coincide with the nutation frequency of a prolate body. This creates a resonance between the systems in which the nutation oscillations and the chamber wave motions feed one another. The energy from the chamber oscillations is stored in the system oscillations

which in turn increases the internal oscillations. The resulting flow is an unsymmetrical flow field accumulated due to the wave motion. (7)

The Composite Flow Field

The combination of these three flows yields what can be called the composite flow field as all of the flow patterns act superimposed on one another as shown in figure 11 above. Understanding the behavior of this complex flow and the effect on the nutation phenomenon requires intense calculations. Through the use of the energy analysis, it is hoped that it can be understood what parameters have a large effect on the occurrence of nutation instabilities without the need for such an in depth analysis. The assumed flow interactions may very well be occurring, but there is still no complete understanding as to why this oscillation only occurs for certain vehicles.

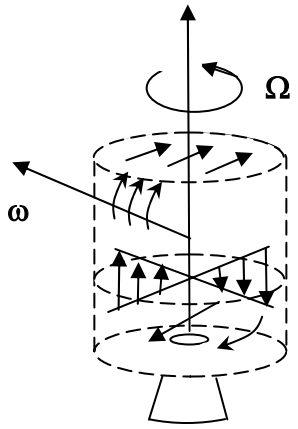

Figure 11 – Composite Flow Field

Dimensionless Variables

Two important dimensionless variables, the residence time and the Rossy number are useful in understanding behavior inside of the spinning rockets. They are also helpful in understanding the importance of changing the size of the vehicle. There are certain characteristic properties used to create these dimensionless variables; they are the characteristic length, speed, and time of the spinning rocket.

The characteristic length, R_0, represents the average chamber radius for a specific burn time. The star propellants burn in a star-like shape, hence the name, and for simplicity, an average chamber radius is used in calculations. The characteristic speed, v_b, represents the typical gas speed in the chamber, the speed of the particles leaving the burning propellant surface. The characteristic time, Ω^{-1}, is the inverse of the vehicle spin rate.

Residence time, τ, is the time required for a particle to transverse the chamber radius.

$$\tau = \frac{R_o}{v_b} \tag{1}$$

The particle stay-time is the dimensionless time, acquired by dividing the residence time by the characteristic time of the rocket.

$$\tau = \frac{R_o \Omega}{v_b} \tag{2}$$

The residence time is helpful in understanding the effect of the Coriolis force on the system. Since the gas is deformable, the effect of the force on the gas changes particle velocities and directions. The assumption of a simplified flow in previous jet damping

models neglected this influence. With the chamber radius as a term in the numerator, it can be seen that a larger rocket chamber will increase the amount of time of a particle's residence within the chamber. In the smaller rockets of previous flights, the flow of gas particles to the nozzle had such a short residence time that there was no noticeable force effect developed from the Coriolis acceleration. However, in a larger rocket with longer lateral dimensions, with the increased residence time, there is a greater time for action of Coriolis forces allowing alteration of the streamlines.

$$\varepsilon = \frac{v_b}{R_o \Omega} \tag{3}$$

It is noticeable to point out that for large particles stay times within the chamber, the Rossy number is small. Evaluation of flight data shows that only spacecraft with small Rossy numbers approaching unity or smaller have experienced propulsion driven nutation. From data, Rossy number can be seen to decrease during burn showing the connection between the growth and the increase in rocket size.

The motor burn time also has an impact on nutation growth since larger motors have increased propellant action times. Therefore, even small disturbances occurring in the gas flow during this increased time have more time to apply a noticeable impact on the system torque. The obvious correlation to increased size only encourages an understanding of possible correlations between sizing and reduction of the occurrence of nutation. With that being said, this leads us to the formulation of the energy dissipation analysis and a possible means of understanding what is exactly is encouraging growth. (6)

CHAPTER 4

Energy Formulation

To understand the kinetic energy effects on nutation growth, it was determined that the vehicle could be treated as a rigid body undergoing loss of mass as propellant is burn. This would have the effect of an energy transfer from the system. To understand the effects that such a loss of energy would produce, it is necessary to discuss previously investigated effects of energy dissipation on the system.

What is Energy Dissipation?

Energy dissipation is generally an elastic body effect resulting from elastic vibrations induced by the body's gyroscopic motion. This dissipation results in a change in the precession coning angle, θ, allowing a small deviation in the precession of the spin axis to continue to grow larger.

A symmetric body of revolution with principle moments of inertia I_1, I_2, I_3 with constant properties, a rigid body, does not have these elastic effects. Therefore, it does not experience dissipative effects in coning angle. If the body experiences no external torque, it maintains steady precession with a constant attitude. If acted upon by a torque, the resulting angle imparted would be maintained instead of growing after its application has ended.

In the case of no energy dissipation, both of the axes of minimum and maximum moment of inertia are considered to be stable; in the case of energy dissipation only the

axis of maximum moment of inertia is stable. When the body spins about the axis of least moment of inertia, the coning can continue as far as to completely change its attitude until the spin is about the axis of greatest inertia. Vehicles with larger lateral moments of inertia compared to the axial spin moment of inertia, such as the slender prolate bodies commonly used in many satellites and missiles, are considered to be inherently unstable. (3)

Dissipation Development

The following formulation has been developed to examine the effect that change in the kinetic energy of the system can have on the nutation angle. Considering a body with elasticity and constant mass properties, the initial formulation is as follows. Since it is being assumed that the system is under zero torque, Euler's dynamic equations show the angular momentum vector **h** to be constant. (3)

$$M_1 = \dot{h}_1 + \omega_2\omega_3(I_3 - I) = 0 \tag{4}$$

$$M_2 = \dot{h}_2 + \omega_1\omega_3(I - I_3) = 0 \tag{5}$$

$$M_3 = \dot{h}_3 + \omega_1\omega_2(I - I) = 0 \tag{6}$$

The angular momentum vector and rotational kinetic energy can be expressed as

$$\vec{H} = I\vec{\omega} = I_1\omega_1 + I_2\omega_2 + I_3\omega_3\,, \tag{7}$$

$$\text{and } T = \frac{1}{2}(I_1\omega_1^2 + I_2\omega_2^2 + I_3\omega_3^2)\,. \tag{8}$$

Remembering $I_1 = I_2 = I$, the square of the angular momentum's magnitude becomes

$$H^2 = I^2(\omega_1^2 + \omega_2^2) + I_3^2\omega_3^2\,. \tag{9}$$

The rotational kinetic energy can be simplified as follows:

$$T = \frac{1}{2}(I(\omega_1^2 + \omega_2^2) + I_3\omega_3^2), \tag{10}$$

$$2T = I_1(\omega_1^2 + \omega_2^2) + I_3\omega_3^2. \tag{11}$$

Multiplying the kinetic energy by I and subtracting from the square of the momentum and simplifying yields

$$H^2 - 2T\,I = I^2(\omega_1^2 + \omega_2^2) + I_3^2\omega_3^2 - I\left(I(\omega_1^2 + \omega_2^2) + I_3^2\omega_3^2\right), \tag{12}$$

$$H^2 - 2T\,I = I_3(I_3 - I)\omega_3^2. \tag{13}$$

From the vector diagram,

$$H = \frac{I_3\omega_3}{\cos\theta}. \tag{14}$$

Rearranging and substituting for ω_3 yields

$$H^2 - 2T\,I = \frac{(I_3 - I)}{I_3}H^2\cos^2\theta. \tag{15}$$

In past literature, the next step has been to take the derivative with mass properties remaining constant yielding the following result.

$$\frac{dT}{dt} = \frac{H^2}{I}\left(\frac{(I_3 - I)}{I_3}\right)(\sin\theta\cos\theta)\dot{\theta} \tag{16}$$

This expression is used to express the nutation angle rate depending on the rate of change of the systems kinetic energy. Depending on the ratio of moments of inertia, with some elastic dissipation of kinetic energy, a negative rate, the nutation rate can be positive or negative.

This result is only valid for an elastic body. It is important that there is an understanding of the behavior of a rigid body before discussing mass transfer effects.

Rigid Body Effects

Through the following analysis of the Euler dynamical equations and the resulting angular rates it can be shown that there is no change in the kinetic energy and therefore no change in nutation for a rigid body.

Expressing the derivative of angular momentum as

$$\dot{h}=I^*\dot{\omega} + \dot{I}^*\omega \ . \tag{17}$$

Constant mass yields a derivative of inertia term of zero so when it is plugged into the Euler equations and they are rearranged they become

$$I^*\dot{\omega}_1 + \omega_2\omega_3(I_3 - I) = 0 , \tag{18}$$

$$I^*\dot{\omega}_2 - \omega_1\omega_3(I_3 - I) = 0 , \tag{19}$$

$$I^*\dot{\omega}_3 = 0 . \tag{20}$$

For simplification the following expression will be used called the nutation frequency.

$$\lambda = \omega_3\left(\frac{I_3 - I}{I}\right) \tag{21}$$

This simplifies the first two equations to

$$\dot{\omega}_1 + \lambda\omega_2 = 0 \tag{22}$$

$$\dot{\omega}_2 - \lambda\omega_1 = 0 . \tag{23}$$

Multiplying these equations through by ω_1 and ω_2 respectively and adding yields

$$\omega_1\dot{\omega}_1 + \omega_2\dot{\omega}_2 = 0 . \tag{24}$$

Equation 20 shows that $\dot{\omega}_3 = 0$.

Taking the time derivative with mass constant yields

$$\frac{dT}{dt} = \frac{d}{dt}\left(\frac{1}{2}(I(\omega_1^2 + \omega_2^2) + I_3\omega_3^2)\right) \tag{25}$$

$$\frac{dT}{dt} = I\left(\omega_1 \frac{d\omega_1}{dt} + \omega_2 \frac{d\omega_2}{dt}\right) + I_3\omega_3 \frac{d\omega_3}{dt} \tag{26}$$

Substituting in equations 20 and 24, it is shown that for a rigid body with constant mass there is no change in the rotational kinetic energy. With no change in kinetic energy, there can be no change in the nutation angle. Therefore, if the body is not assumed to be undergoing elastic effects, something else that can cause a change of energy must be taken into consideration.

Before moving on with the formulation, the derivation of the solution for the angular rates for a rigid body will be discussed for later comparison with actual observed angular rate behavior.

Rigid Body Angular Rates

The solution obtained shows that there is no change in the magnitude of the pitch and yaw angular velocities. The spin rate remains constant as shown earlier. This is not what occurs in reality or in the case considered in modeling the energy formulation. Growth in the angular rates encourages deviation in the nutation angle. With no growth in the angular rates for the rigid case, there is no growth in the nutation angle. (3)

Remembering the equations derived from the basic Euler equations,

$$\dot{\omega}_1 + \lambda\omega_2 = 0 \tag{27}$$

$$\dot{\omega}_2 - \lambda\omega_1 = 0 \tag{28}$$

and then differentiating (28) and substituting from (27) yields

$$\ddot{\omega}_1 + \lambda^2\dot{\omega}_1 = 0\,. \tag{29}$$

This is a simple second-order homogeneous equation that can be solved for the following sinusoidal solution

$$\omega_1 = a\cos(\lambda t) + b\sin(\lambda t)\,. \tag{30}$$

Solving for the multiplication constants,

$$\omega_1(0) = a\cos(\lambda \cdot 0) + b\sin(\lambda \cdot 0) = a \tag{31}$$

$$\dot{\omega}_1(0) = -a\lambda\sin(\lambda \cdot 0) + b\lambda\cos(\lambda \cdot 0) = b, \text{ therefore } b = \frac{\dot{\omega}_1(0)}{\lambda} \tag{32}$$

yields

$$\omega_1 = \omega_1(0)\cos(\lambda t) + \frac{\dot{\omega}_1(0)}{\lambda}\sin(\lambda t)\,. \tag{33}$$

Rearrange equation (28) to solve for the yaw angular rate.

$$\omega_2 = \frac{-\dot{\omega}_1}{\lambda} \tag{34}$$

Differentiating the pitch rate and substituting

$$\dot{\omega}_1 = -a\lambda\sin(\lambda t) + b\lambda\cos(\lambda t) \tag{35}$$

yields

$$\omega_2 = -a\sin(\lambda t) + b\cos(\lambda t) \tag{36}$$

and plugging in for the constants yields

$$\omega_2 = \omega_1(0)\sin\lambda t - \frac{\dot{\omega}_1(0)}{\lambda}\cos\lambda t\,. \tag{37}$$

These equations for angular velocities were developed for the case of a rigid body of constant mass properties. Their constants are dependant on the initial conditions of the pitch rate. This shows that for such a body in which the nutation frequency remains constant due to constant mass and spin rate, the pitch and yaw angular rates maintain constant amplitude.

Energy Transfer

The approach to be taken from this point in the formulation is that of a rigid body undergoing loss of mass; with this loss of mass, the vehicle also experiences the effect of jet damping. The rate of change of the body's kinetic energy is no longer zero; it is decreasing due to the loss of mass. In this analysis, nothing is held constant when the derivative is taken. Therefore, with dissipating rotational kinetic energy, this modified approach to the energy dissipation result can be used to show that there will be an observed change in nutation rate.

Since the body undergoes a loss of mass and therefore jet damping effect, the Euler dynamical equations are represented by the following formulation. (3)

$M = \dot{h} + \omega \times h$ + rate of change of angular momentum transfer from variable mass system

Still assuming no external toque is applied to the vehicle, the three Euler equations become

$$M_1 = \dot{h}_1 + \omega_2\omega_3(I_3 - I) + \dot{m}l^2\omega_1 = 0 \tag{38}$$

$$M_2 = \dot{h}_2 + \omega_1\omega_3(I - I_3) + \dot{m}\, l^2\omega_2 = 0 \tag{39}$$

$$M_3 = \dot{h}_3 + \omega_1\omega_2(I - I) = 0 \tag{40}$$

Rearranging and simplifying for $\dot{h}$ yields,

$$\dot{h}_1 = -\dot{m}l^2\omega_1 - \omega_2\omega_3(I_3 - I) \tag{41}$$

$$\dot{h}_2 = -\dot{m}l^2\omega_2 - \omega_1\omega_3(I - I_3) \tag{42}$$

$$\dot{h}_3 = 0 \tag{43}$$

Since we are using the magnitude of the angular momentum, the component derivatives can be summed and simplified as follows.

$$\frac{dH}{dt} = \dot{h}_1 + \dot{h}_2 + \dot{h}_3 \tag{44}$$

$$\frac{dH}{dt} = -\dot{m}l^2(\omega_1 + \omega_2) - \omega_3(I - I_3)(\omega_2 - \omega_1) \tag{45}$$

Although the angle may be changing, at each instant in time the vector diagram still holds the same relationship for the magnitude of the angular momentum vector.

$$H = \frac{I_3\omega_3}{\cos\theta} \tag{46}$$

Therefore, the same approach is followed to yield the equation

$$H^2 - 2T\,I = \frac{(I_3 - I)}{I_3}H^2\cos^2\theta\,. \tag{47}$$

However, at this point, the time derivative is taken with mass changing

$$\frac{d}{dt}\left(H^2 - 2T\,I\right) = \frac{d}{dt}\left(\frac{(I_3 - I)}{I_3}H^2\cos^2\theta\right). \tag{48}$$

The result yields a much larger equation that needs to be arranged and simplified to solve.

$$2H\frac{dH}{dt} - \left(2T\frac{dH}{dt} + 2I\frac{dI}{dt}\right) = \tag{49}$$

$$\left[\left(\frac{I_3\frac{dI_3}{dt}-I_3\frac{dI}{dt}}{I_3^2}\right)-\left(\frac{I_3\frac{dI}{dt}-I\frac{dI_3}{dt}}{I_3^2}\right)\right]H^2\cos^2\theta+\left(\frac{(I_3-I)}{I_3}\right)\left(2H\frac{dH}{dt}\right)\cos^2\theta+\left(\frac{(I_3-I)}{I_3}\right)H^2(-2\sin\theta\cos\theta\dot{\theta})$$

The equation is thus simplified

$$-2I\frac{dT}{dt}=\left\{\begin{array}{l}2T\frac{dI}{dt}-\frac{d}{dt}\left(\frac{I}{I_3}\right)H^2\cos^2\theta\\ +\left(-2H\frac{dH}{dt}+\left(\frac{(I_3-I)}{I_3}\right)\left(2H\frac{dH}{dt}\right)\cos^2\theta\right)\\ +\left(\frac{(I_3-I)}{I_3}\right)H^2(-2\sin\theta\cos\theta\dot{\theta})\end{array}\right\} \tag{50}$$

and rearranged to obtain an expression for the change in kinetic energy.

$$\frac{dT}{dt}=\left\{\begin{array}{l}-\frac{T}{I}\frac{dI}{dt}+\frac{d}{dt}\left(\frac{I}{I_3}\right)\frac{H^2}{2I}\cos^2\theta\\ +\left(1-\left(\frac{I_3-I}{I_3}\right)\cos^2\theta\right)\frac{H}{I}\frac{dH}{dt}\\ +\left(\frac{I_3-I}{I_3}\right)\frac{H^2}{I}(\sin\theta\cos\theta\dot{\theta})\end{array}\right\} \tag{51}$$

This is the extended form of the energy dissipation equation. To directly show the effect of the systems decrease in kinetic energy on the coning angle, it must be set equivalent to some rate of change of kinetic energy. Going back to the definition of rotational kinetic energy, the time derivative with non-constant mass properties is taken.

It is then set equivalent to equation 51. The angular rate can then be solved for through simplifications and rearrangement as follows.

Again, the rotational kinetic energy is expressed as

$$T = \frac{1}{2}(I_1\omega_1^2 + I_2\omega_2^2 + I_3\omega_3^2)\,. \tag{52}$$

Taking the time derivative,

$$\frac{dT}{dt} = \frac{d}{dt}\left(\frac{1}{2}(I(\omega_1^2 + \omega_2^2) + I_3\omega_3^2)\right) \tag{53}$$

$$\frac{dT}{dt} = \frac{dI}{dt}\frac{(\omega_1^2 + \omega_2^2)}{2} + I\left(\omega_1\frac{d\omega_1}{dt} + \omega_2\frac{d\omega_2}{dt}\right) + I_3\omega_3\frac{d\omega_3}{dt} + \frac{dI_3}{dt}\frac{\omega_3^2}{2} \tag{54}$$

setting the time derivatives of energy equal to each other

$$-\frac{T}{I}\frac{dI}{dt} + \left(1 - \left(\frac{I_3 - I}{I_3}\right)\cos^2\theta\right)\frac{H}{I}\frac{dH}{dt} + \frac{d}{dt}\left(\frac{I}{I_3}\right)\frac{H^2}{2I}\cos^2\theta + \left(\frac{I_3 - I}{I_3}\right)\frac{H^2}{I}(\sin\theta\cos\theta\dot{\theta}) =$$

$$\frac{dI}{dt}\frac{(\omega_1^2 + \omega_2^2)}{2} + I\left(\omega_1\frac{d\omega_1}{dt} + \omega_2\frac{d\omega_2}{dt}\right) + I_3\omega_3\frac{d\omega_3}{dt} + \frac{dI_3}{dt}\frac{\omega_3^2}{2} \tag{54}$$

and rearranging to solve for the nutation rate

$$\left(\frac{I_3 - I}{I_3}\right)\frac{H^2}{I}(\sin\theta\cos\theta\dot{\theta}) = \frac{T}{I}\frac{dI}{dt} - \left(1 - \left(\frac{I_3 - I}{I_3}\right)\cos^2\theta\right)\frac{H}{I}\frac{dH}{dt}$$

$$-\frac{d}{dt}\left(\frac{I}{I_3}\right)\frac{H^2}{2I}\cos^2\theta + \frac{dI}{dt}\frac{(\omega_1^2 + \omega_2^2)}{2} + I\left(\omega_1\frac{d\omega_1}{dt} + \omega_2\frac{d\omega_2}{dt}\right) + I_3\omega_3\frac{d\omega_3}{dt} + \frac{dI_3}{dt}\frac{\omega_3^2}{2} \tag{55}$$

yields the time rate of change of the nutation angle.

$$\dot{\theta} = \left(\frac{1}{\left(\frac{I_3 - I}{I_3} \right) \frac{H^2}{I} (\sin\theta \cos\theta)} \right) \times \left\{ \begin{array}{l} \frac{T}{I} \frac{dI}{dt} - \left(1 - \left(\frac{I_3 - I}{I_3} \right) \cos^2\theta \right) \frac{H}{I} \frac{dH}{dt} \\ -\frac{d}{dt} \left(\frac{I}{I_3} \right) \frac{H^2}{2I} \cos^2\theta + \frac{dI}{dt} \frac{(\omega_1^2 + \omega_2^2)}{2} \\ + I \left(\omega_1 \frac{d\omega_1}{dt} + \omega_2 \frac{d\omega_2}{dt} \right) + I_3 \omega_3 \frac{d\omega_3}{dt} + \frac{dI_3}{dt} \frac{\omega_3^2}{2} \end{array} \right\} \quad (56)$$

This equation calculates nutation change for a body with no external torques undergoing change in mass and experiencing jet damping effects. It can be analyzed to observe the development of coning behavior in various flight vehicles. Through testing variations of parameters, their relative effects on coning behavior can be determined.

CHAPTER 5

Analysis

The equation representing the rate of change of the nutation angle is first-order nonlinear; the unknown to be solved for is contained within the equation to be solved. Such a problem needs to be solved using the numerical convergence technique.

Numerical Technique

The fourth order Runge-Kutta is a commonly used numerical method for obtaining approximate solutions to first-order equations given some initial value of the dependent variable. The procedure uses an approximation to a Taylor polynomial of degree four to add incremental values to the value of the variable for each time step. To analyze over a long period of time, this calculation is intensive and requires computer calculation. MATLAB programming software is suited for the calculations needed. A program was written using a built-in fourth order solver to perform the analysis of the problem.

Two vehicles, the Intelsat VI and the Westar V, were used as a main focus in the analysis of the coning behavior. Empirical equations from curve-fits of data points for the lateral moment of inertia, roll moment of inertia, mass flow, chamber radius, and center of gravity position from both vehicles were used in the program. The following figures show these parameters for both vehicles; several features of each differ and have differing effects on the resulting nutation growth rate for the vehicles and thus require discussion.

Vehicles undergoing loss of mass in turn experience decreasing system moments of inertia. Figures 12-15 show comparisons of the lateral and roll moments of inertia for both the Westar V and Intelsat VI vehicles. Though both vehicles have very similar sizing dimensions, the Westar has an initial weight of 1280 lbs and the Intelsat VI had an initial weight of 4202 lbs. (8) As seen in the following figures, the Intelsat VI has much larger moments of inertia compared to the Westar.

The vehicles in question are of the prolate shape, lending towards their instability about their spin axis of smaller inertia as discussed earlier. The smaller magnitude of the chamber radius versus the center of gravity position is apparent in figures 16-19. It can be seen that as motor burn progresses, the magnitude of the center of gravity position changes more rapidly than smaller chamber radius. As a result, although both vehicles start off with a much larger lateral moment of inertia than that about the roll axis, towards the end of burn, the lateral moments have rapidly decreased to approach similar values of inertia as those of the roll inertia as the following figures show.

Figures 20 and 21 show the change in mass flow rate with time for both vehicles; it appears that the intensity of the coning is closely related. The mass flow rate of the Westar is approximately three times less than the Intelsat more than two thirds of the burn. However, whereas the Intelsat's flow shows a parabolic growth then decreases to zero, the Westar shows a small continued growth throughout burn. Without looking at the result of the programming, it would be a logical assumption that the coning in the Intelsat would decrease towards the end of burn while the Westar oscillations would just cease upon completion of burn. The parabolic flow rate during Intelsat burn also suggests that their may be such a growth in coning relative to the initial and final angles.

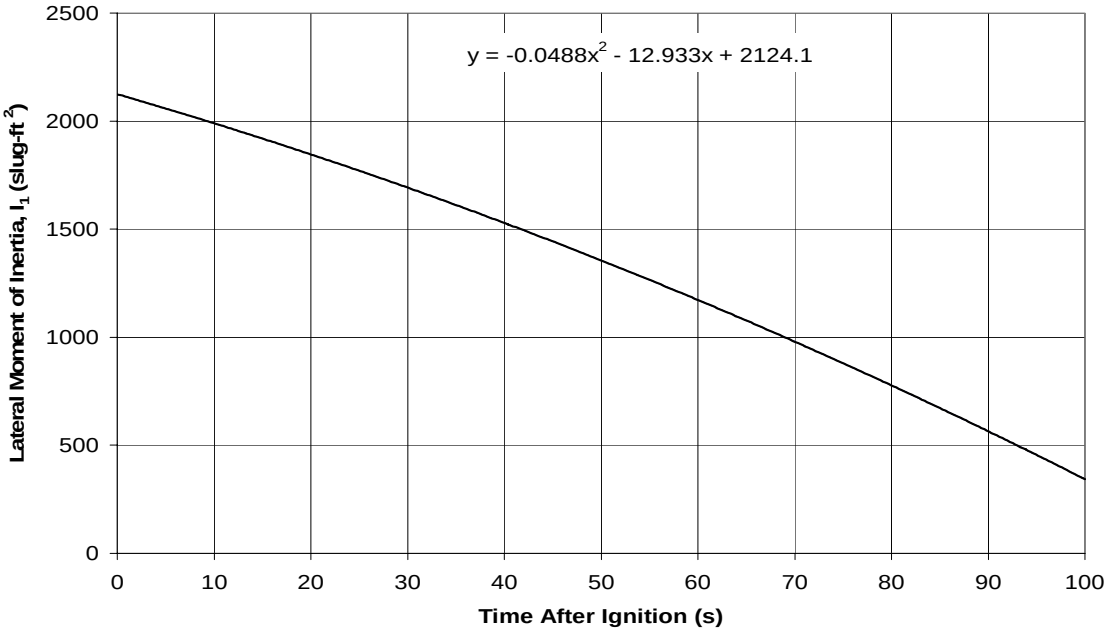

Figure 12 - Lateral Moment of Inertia vs. Time (Westar V)

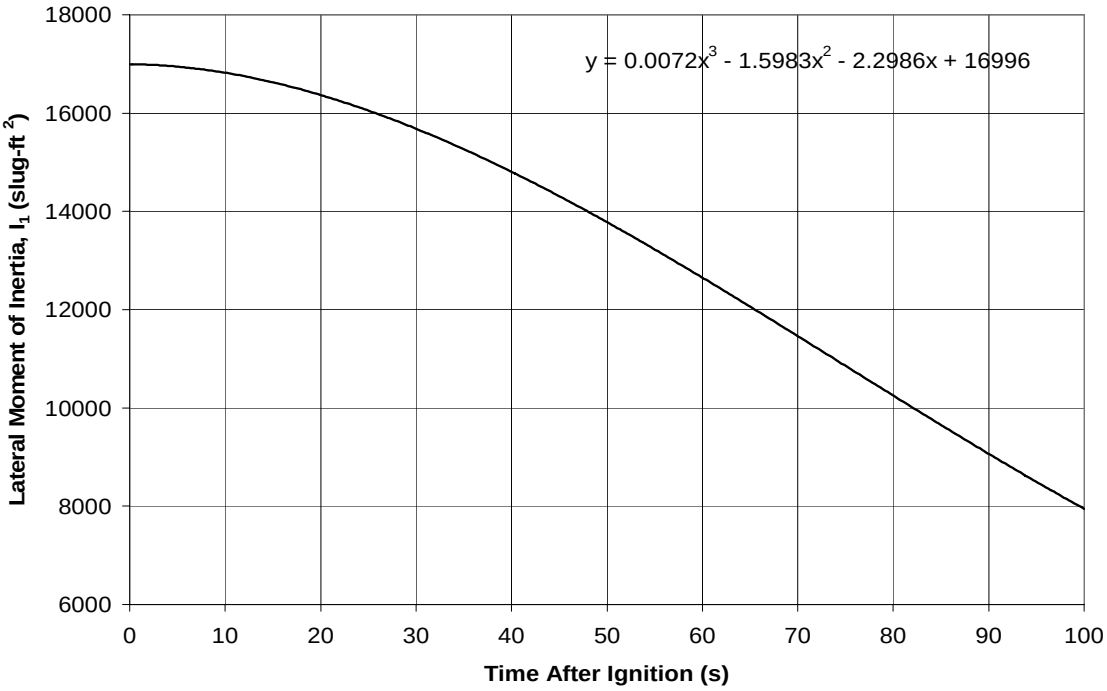

Figure 13 - Lateral Moment of Inertia vs. Time (Intelsat VI)

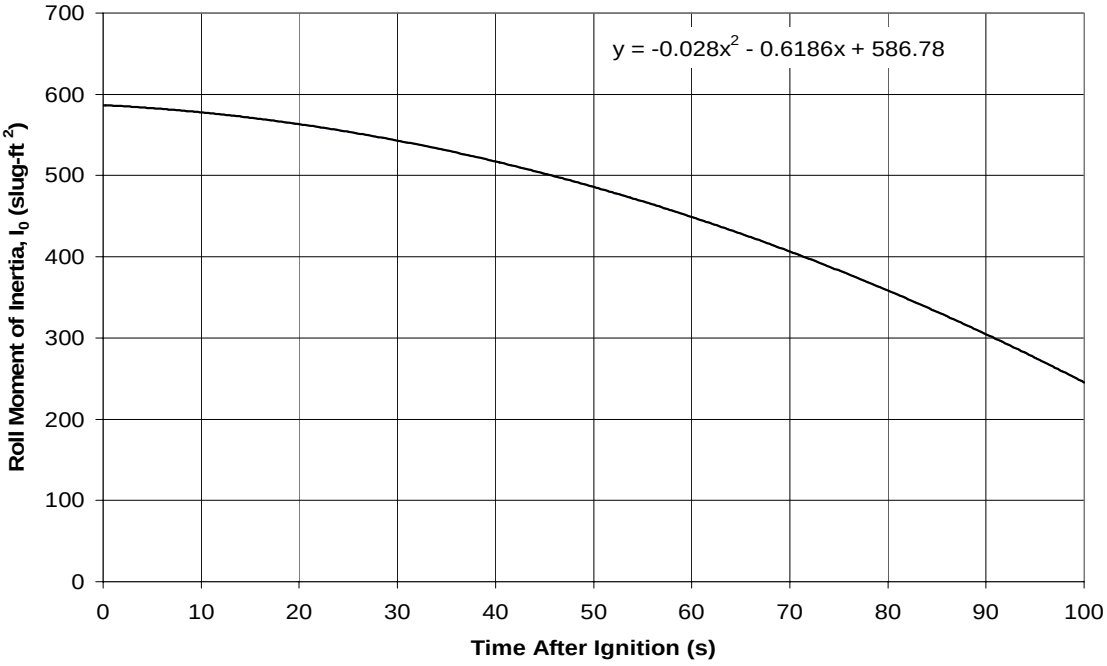

Figure 14 - Roll Moment of Inertia vs. Time (Westar V)

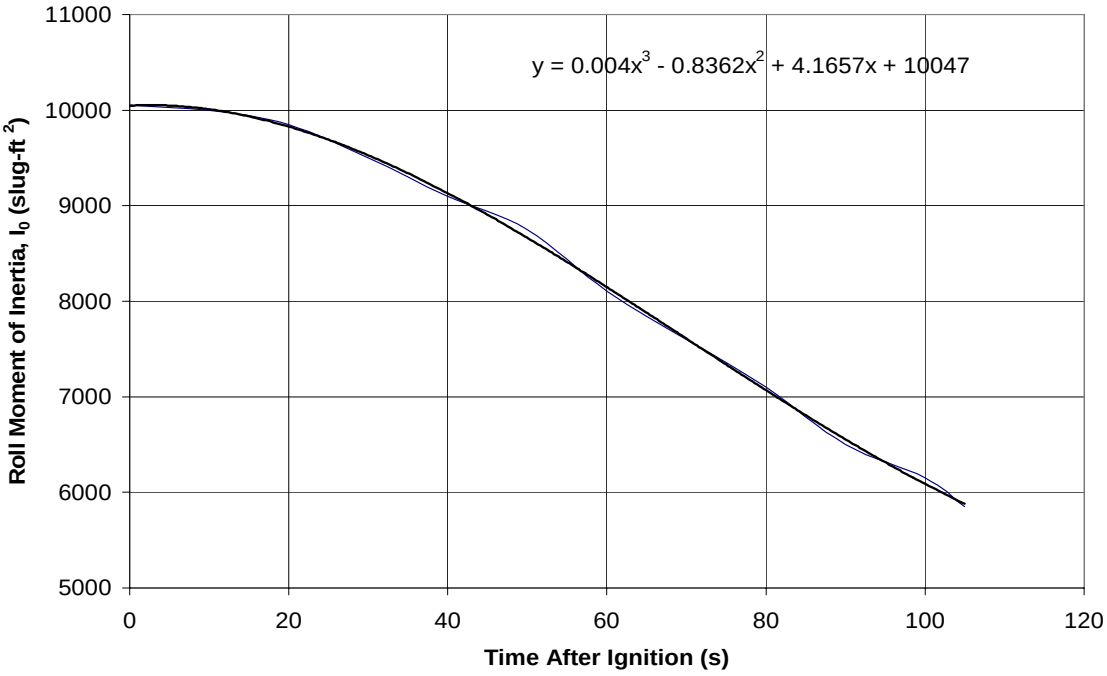

Figure 15 - Roll Moment of Inertia vs. Time (Intelsat VI)

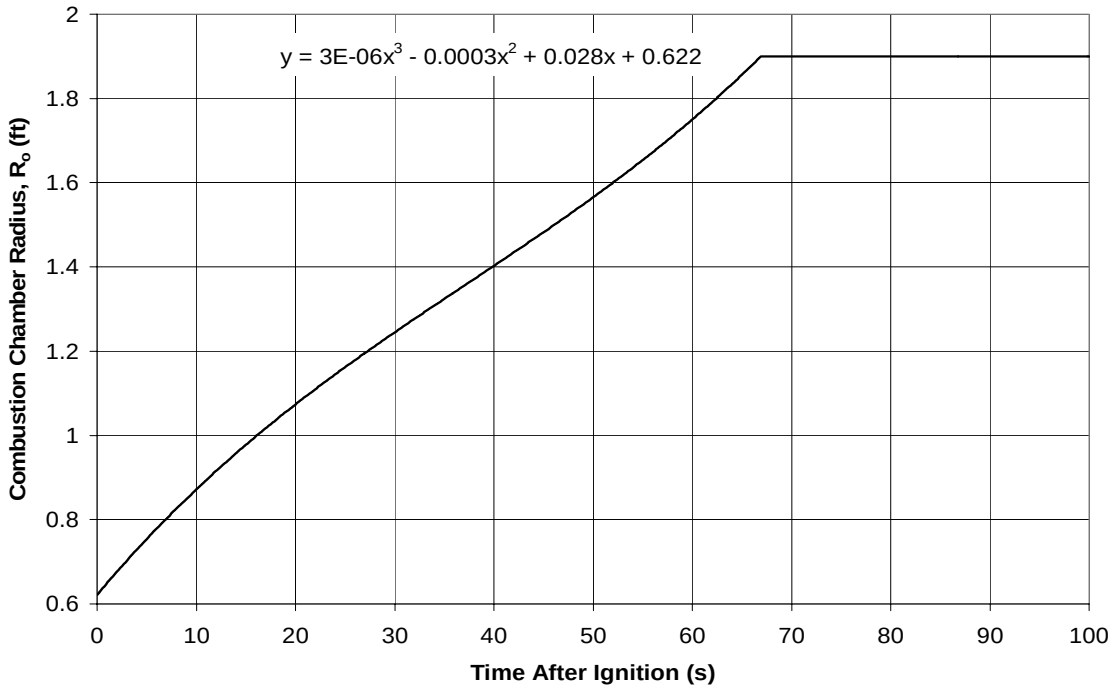

Figure 16 - Average Combustion Chamber Radius vs. Time (Westar V)

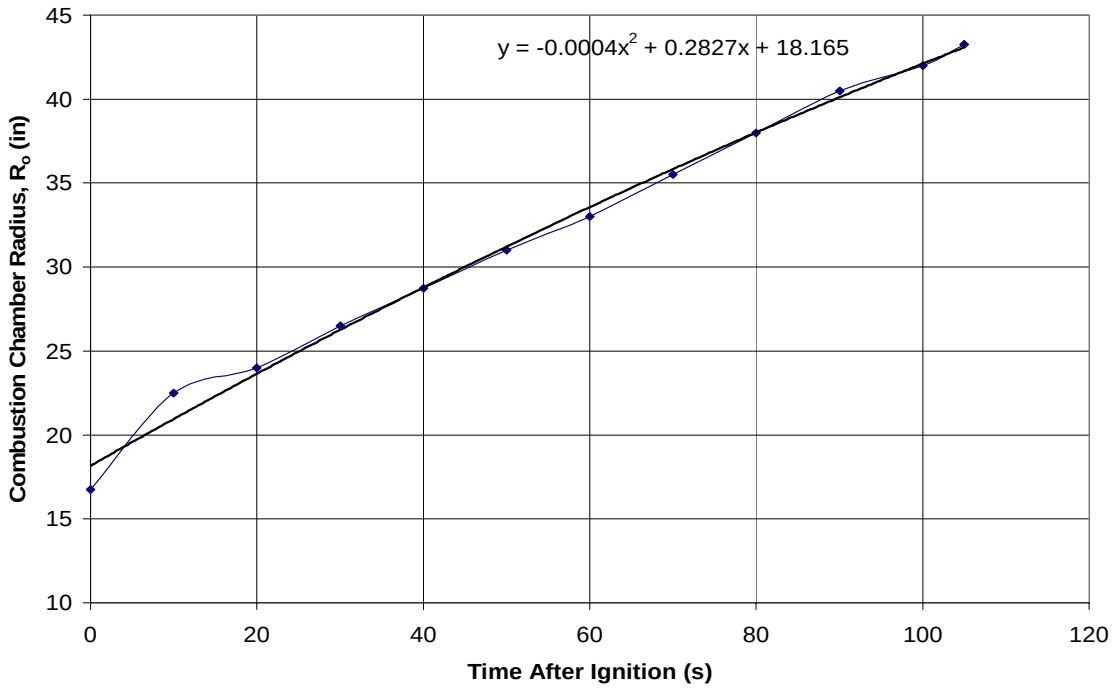

Figure 17 - Average Combustion Chamber Radius vs. Time (Intelsat VI)

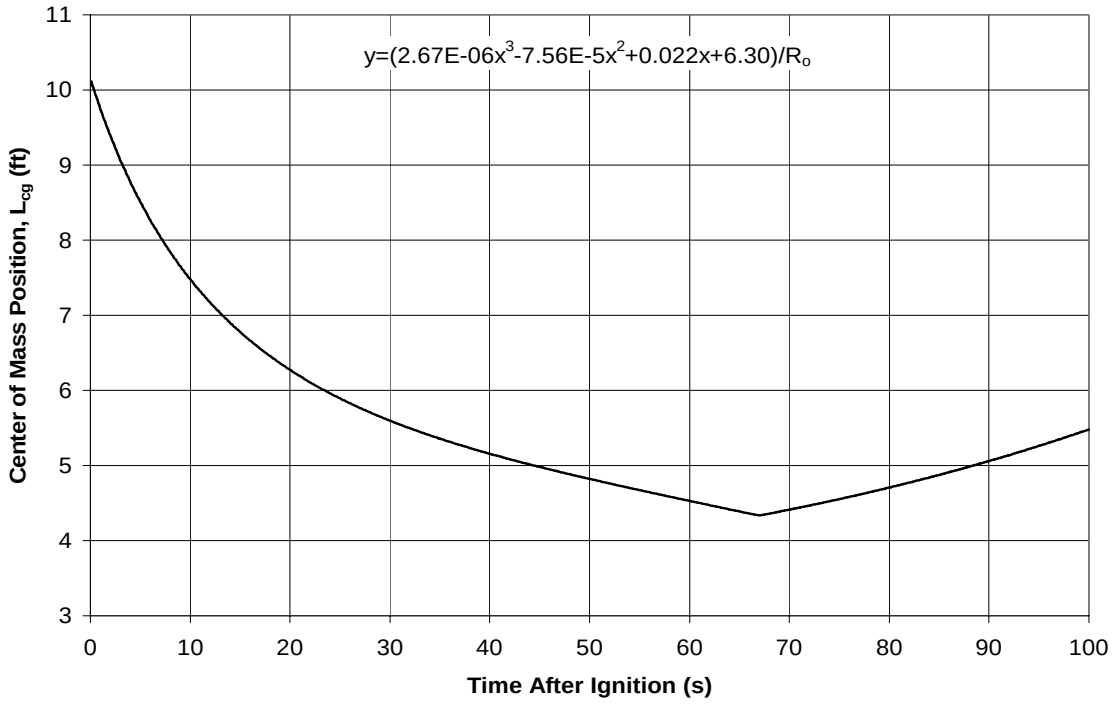

Figure 18 - Center of Gravity Position vs. Time (Westar V)

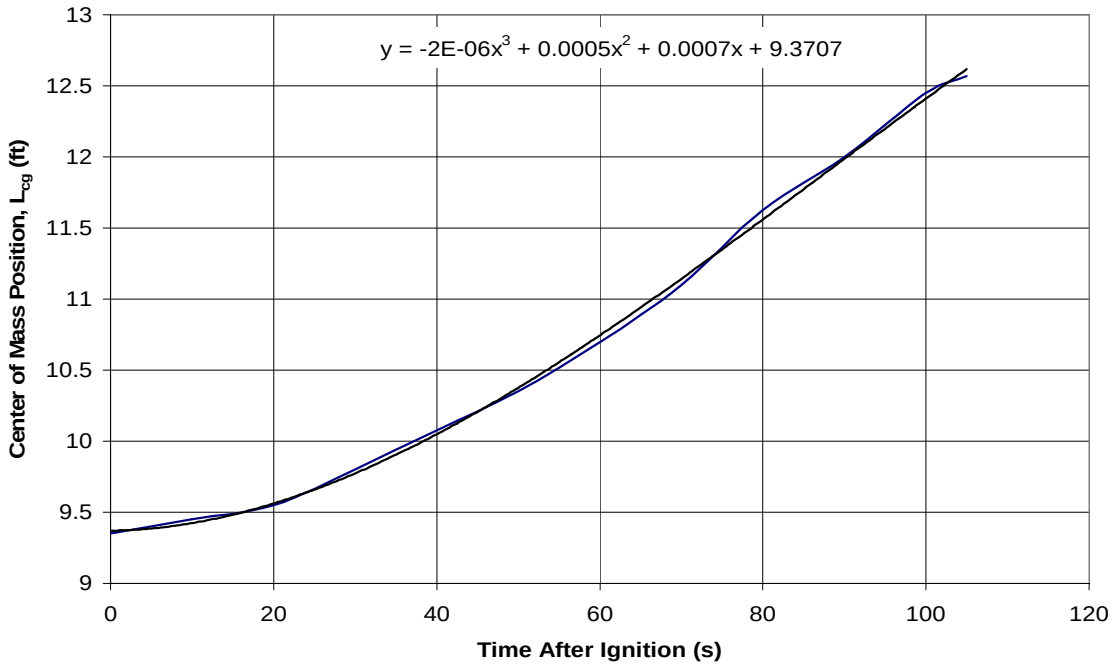

Figure 19 - Center of Gravity Position vs. Time (Intelsat VI)

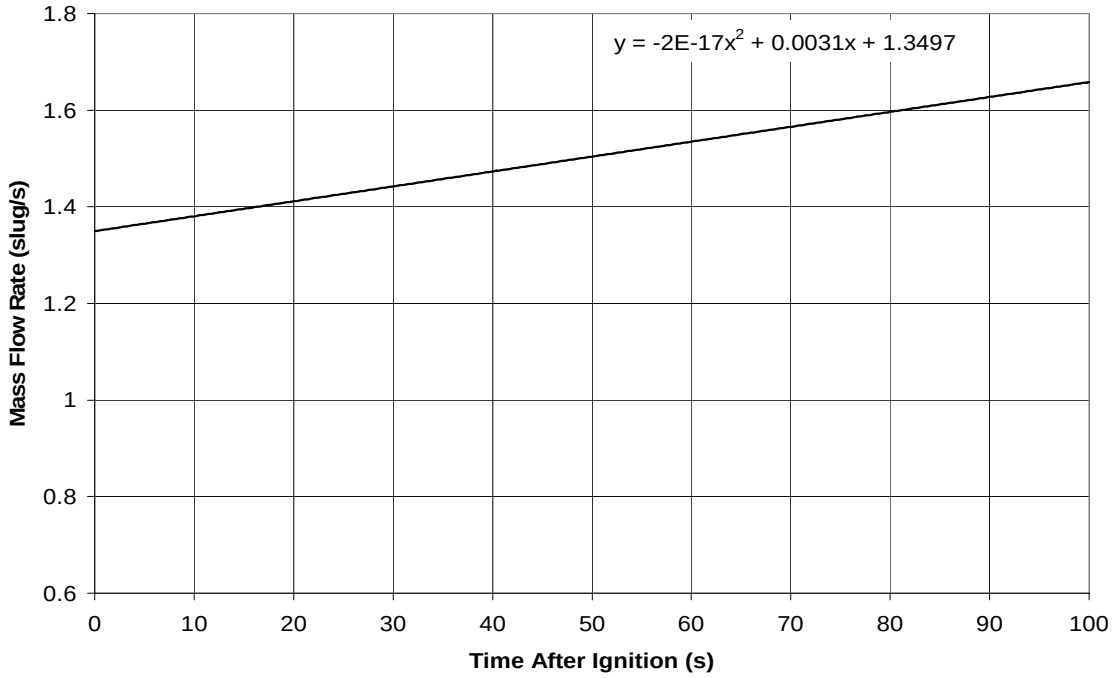

Figure 20 - Mass Flow Rate vs. Time (Westar V)

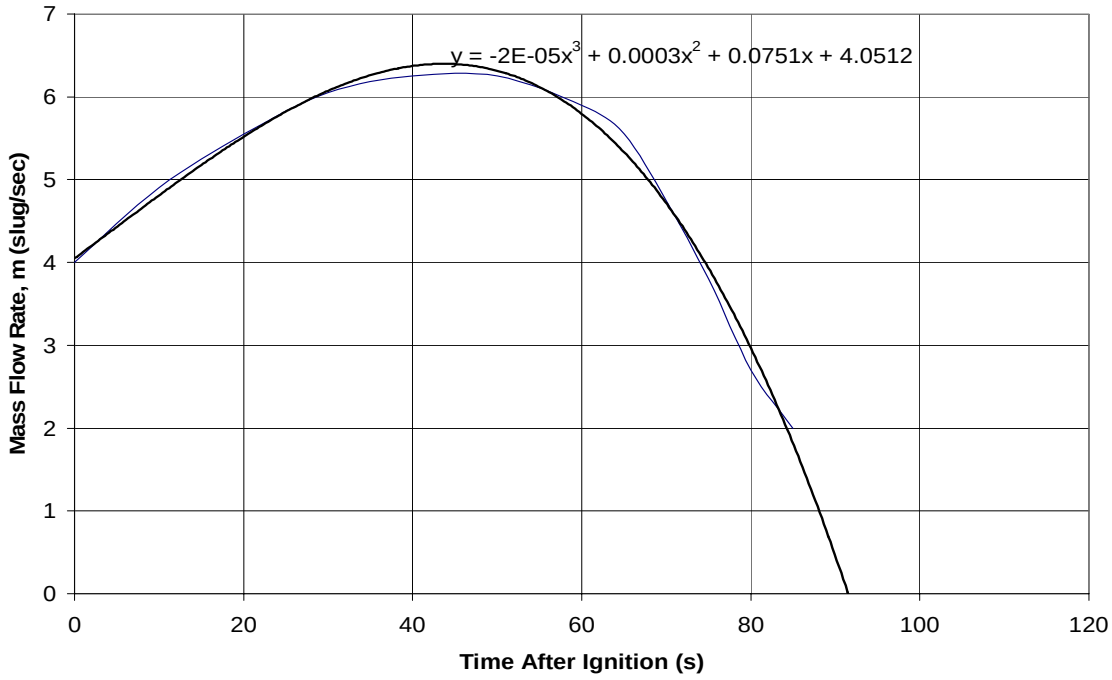

Figure 21 - Mass Flow Rate vs. Time (Intelsat VI)

Both vehicles have decreasing frequencies throughout burn as seen in figures 22 and 23. The nutation frequency for the Westar can be seen to be greater than the Intelsat throughout burn. The Rossy number for both vehicles also decreases for both vehicles as seen in figure 24. They are small; remember that this indicates a larger stay time since the Rossy number is the inverse of the residence time. It appears that the Intelsat's Rossy number becomes smaller than the Westar's. This makes sense since the vehicles center of gravity moves farther away from the nozzle indicating that particles would have a larger particle stay-time. If the mass flow rate of the Intelsat did not decrease towards the end of burn, the final nutation growth for this vehicle would most likely be much larger than the Westar final nutation growth.

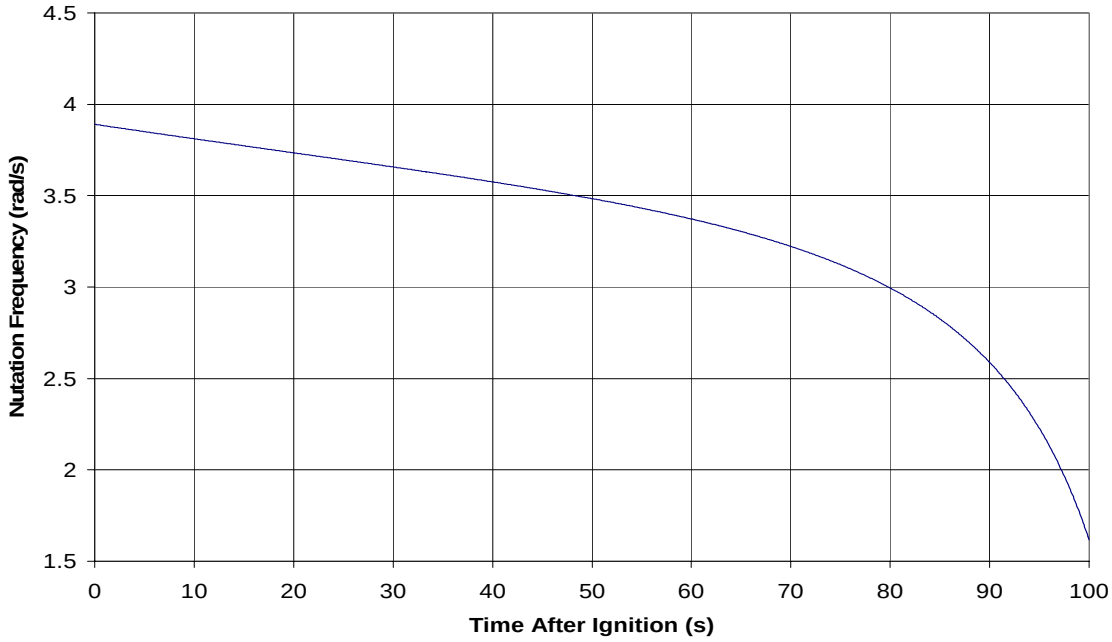

Figure 22 - Nutation Frequency vs. Time (Westar V)

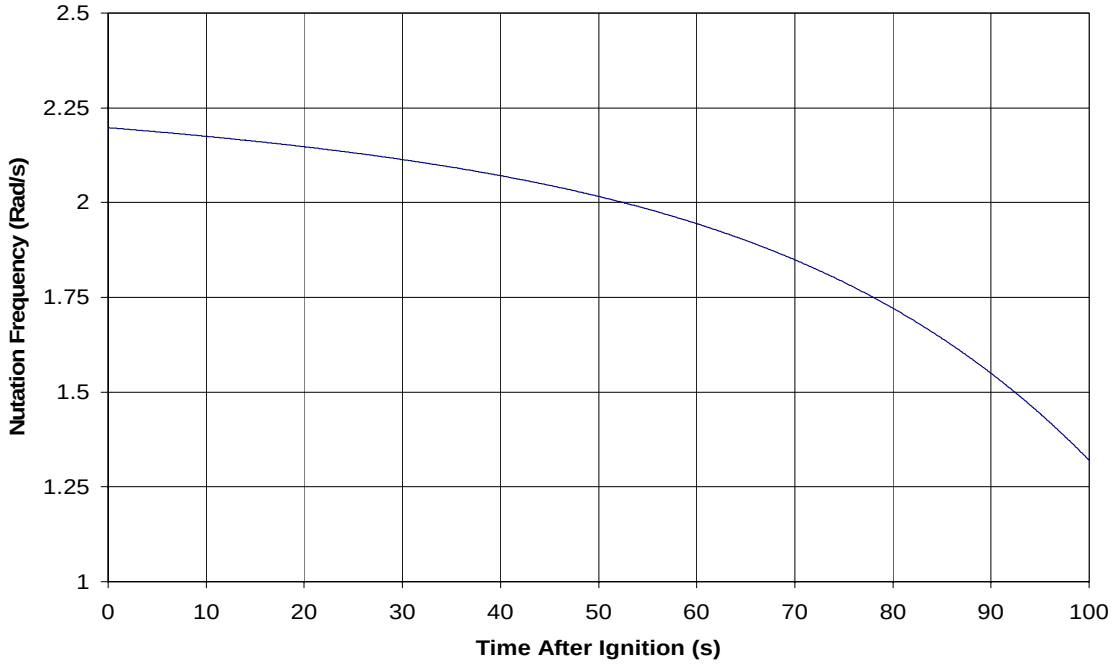

Figure 23 - Nutation Frequency vs. Time (Intelsat VI)

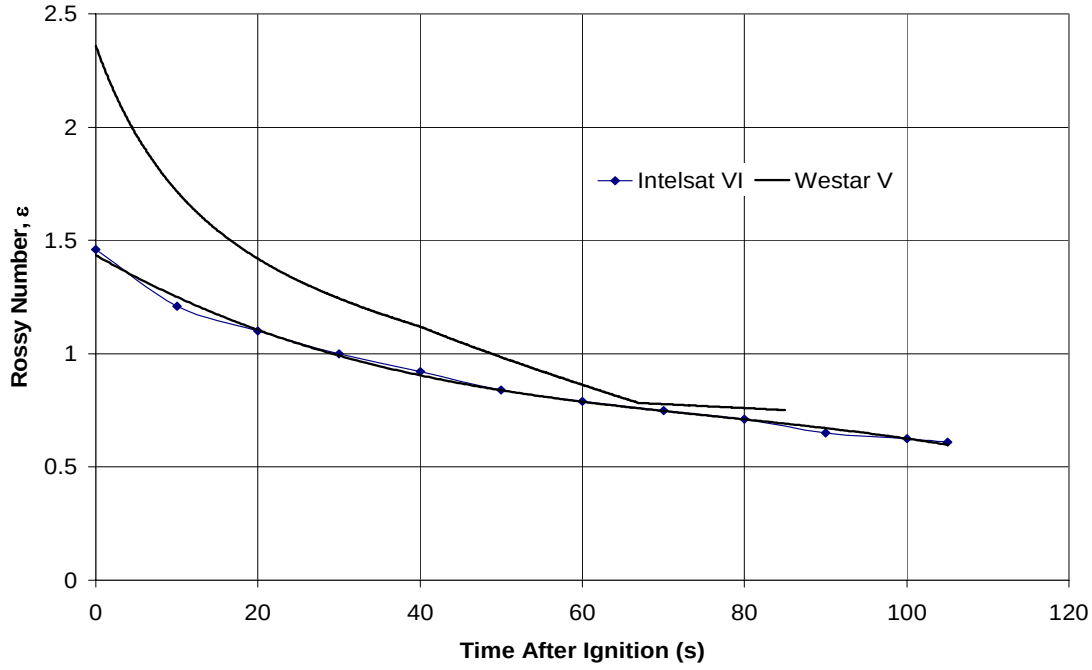

Figure 24 - Rossy Number vs. Time

Analysis of Program Results

The previously discussed vehicle characteristics were used in MATLAB programs that can be found in appendix A to calculate the pitch, yaw, and spin rates and the change of nutation angle.

There is a brief explanation as to the origin of the formulas used to solve for the angular rates in the program. There is no detail as for a rigid body as their solution is not so straight forward and is solved within the code.

Using the previously rearranged Euler equations that have been solved for the change in angular momentum with jet damping,

$$\dot{h}_1 = -\dot{m}l^2\omega_1 - \omega_2\omega_3(I_3 - I) \tag{57}$$

$$\dot{h}_2 = -\dot{m}l^2\omega_2 - \omega_1\omega_3(I - I_3) \tag{58}$$

$$\dot{h}_3 = 0 \tag{59}$$

then substituting in the definition of the angular momentum,

$$I_1*\dot{\omega}_1 + \dot{I}_1*\omega_1 = -\dot{m}l^2\omega_1 - \omega_2\omega_3(I_3 - I) \tag{60}$$

$$I_2*\dot{\omega}_2 + \dot{I}_2*\omega_2 = -\dot{m}l^2\omega_2 - \omega_1\omega_3(I - I_3) \tag{61}$$

$$I_3*\dot{\omega}_3 + \dot{I}_3*\omega_3 = 0 \tag{62}$$

the equations can then be rearranged to solve for the rate of change of the angular rates.

$$\dot{\omega}_1 = \frac{-\dot{m}l^2\omega_1 - \omega_2\omega_3(I_3 - I) - \dot{I}_1*\omega_1}{I_1} \tag{63}$$

$$\dot{\omega}_2 = \frac{-\dot{m}l^2\omega_2 - \omega_1\omega_3(I - I_3) - \dot{I}_2*\omega_2}{I_2} \tag{64}$$

$$\dot{\omega}_3 = \frac{-\dot{I}_3 * \omega_3}{I_3} \tag{65}$$

These equations are also first-degree nonlinear, and are incorporated into the Runge-Kutta solver to obtain their solutions. Their solution is necessary before solving for the coning angle as all of the terms in its equation have some angular rate dependence.

The following figures show the changes in angular rates for the Westar and Intelsat vehicles. The pitch and yaw rates of both vehicles are ninety degrees out of phase with pitch leading. Unlike the rigid body, the pitch and yaw rates undergo changes in amplitude during burn while the spin rate has a slight linear increase.

Figures 25 and 26 show the change in pitch and yaw angular rates for the Westar V. Both rates continue to grow throughout burn until motor cutoff. The increasing mass flow rate for the Westar appears to encourage the continued growth. The predicted behavior of the angular rates closely resembles actual experimental data recorded for the Westar V in both magnitude and growth trend. This measured growth rate can be seen in figure 27.

The Intelsat VI pitch and yaw angular rates can be seen in figures 28 and 29. As can be seen the angular rates increase and then decrease towards the end of motor burn. The time after ignition is carried out to 200 seconds. After propellant burn ceases, without loss of mass to affect the energy, effects on nutation cease as well. The angular velocities take on the behavior of a rigid body with constant amplitude. The growth trend seen during burn also shows the dependence of the angular rates on the mass flow rate of the vehicle.

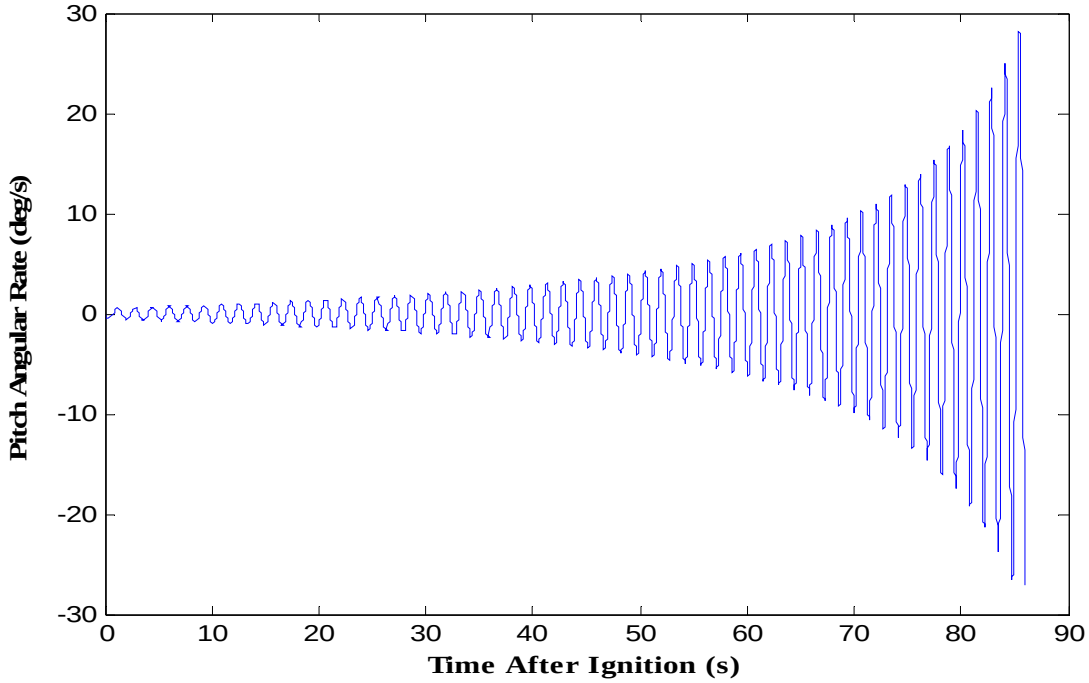

Figure 25 – Pitch Angular Rate vs. Time - Predicted (Westar V)

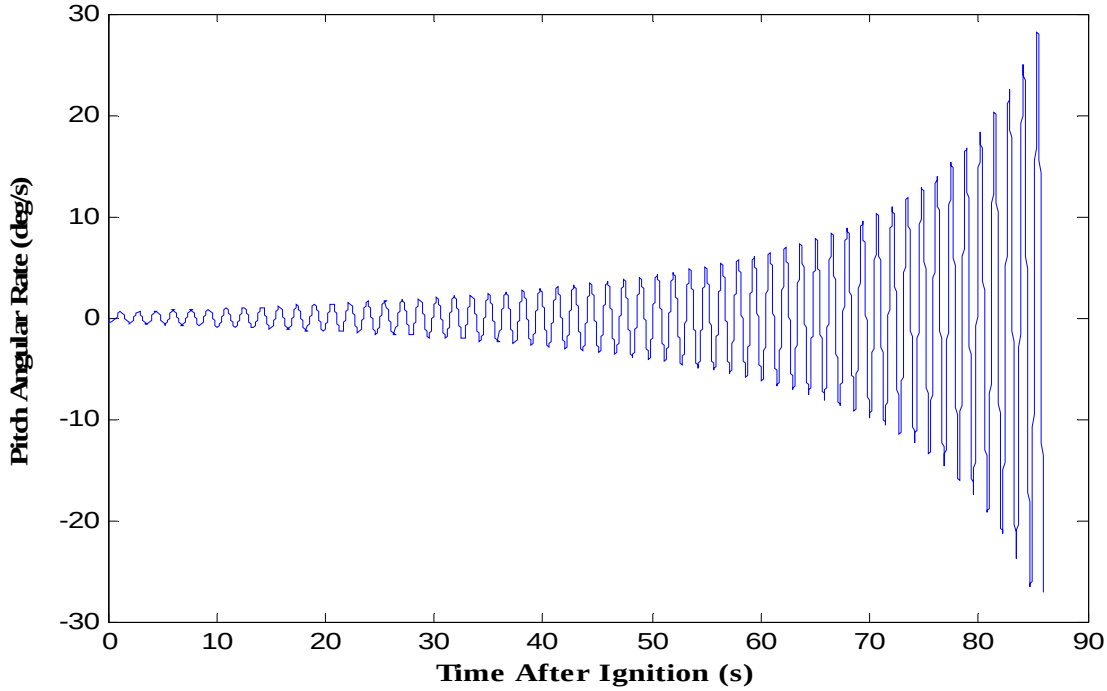

Figure 26 – Yaw Angular Rate vs. Time

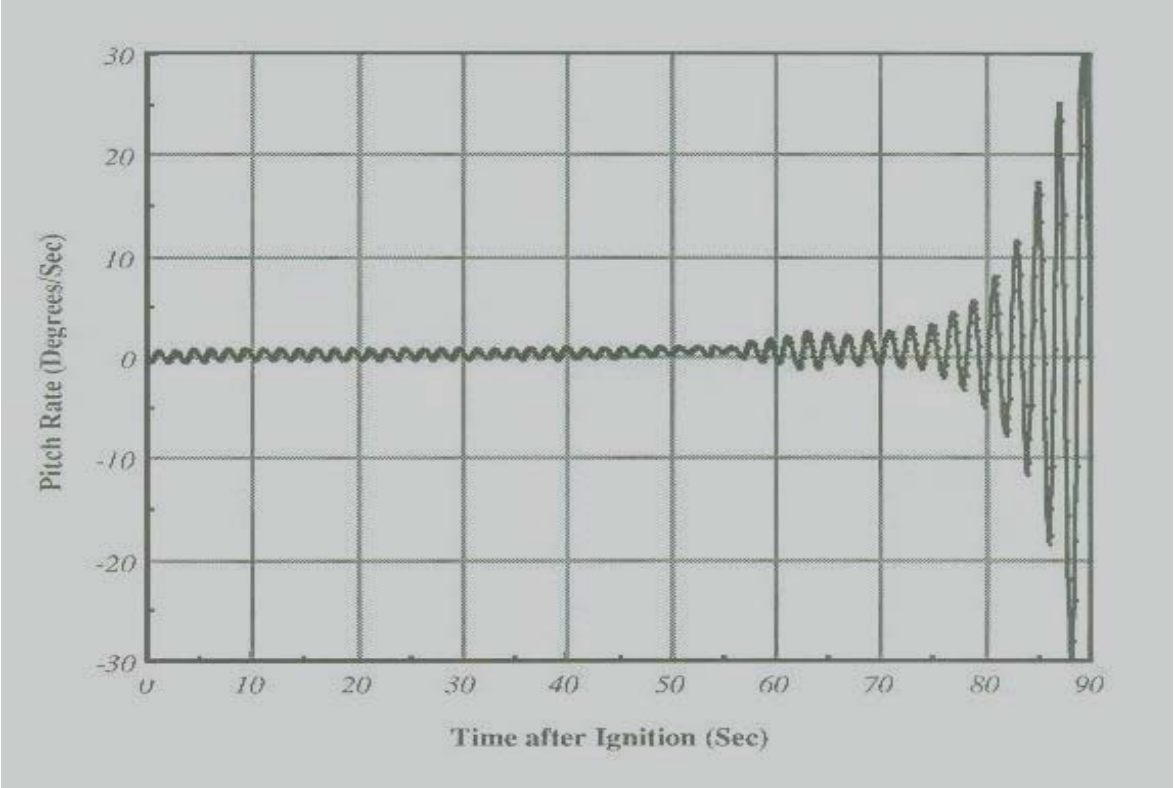

Figure 27 – Pitch Rate vs. Time – Measured (Westar V)

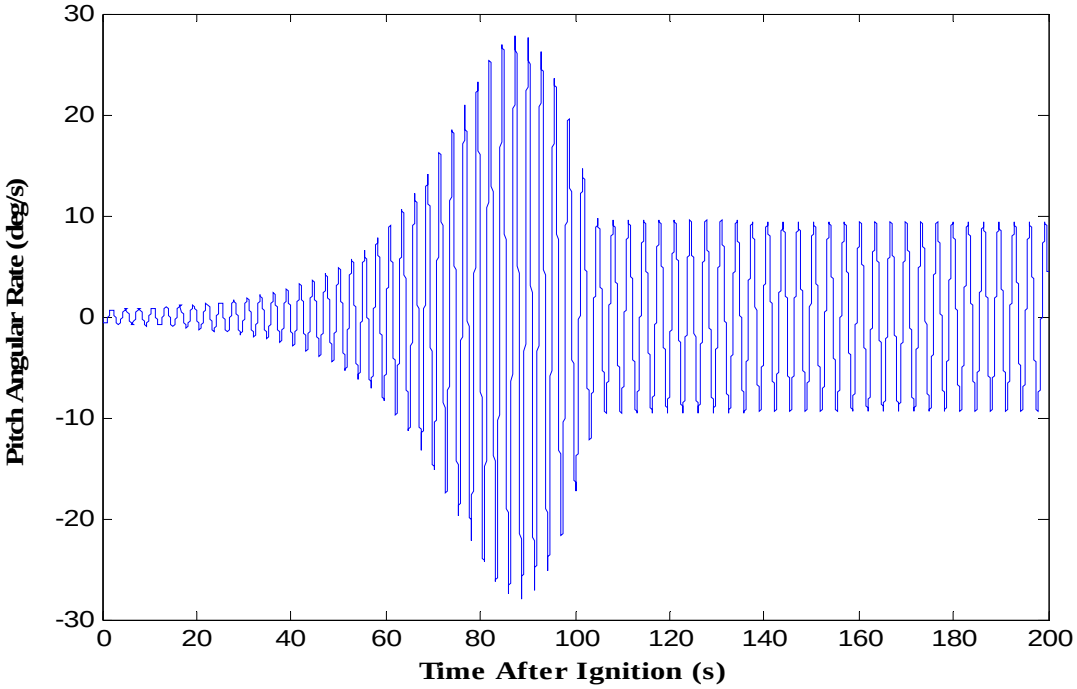

Figure 28 – Pitch Angular Rate vs. Time (Intelsat VI)

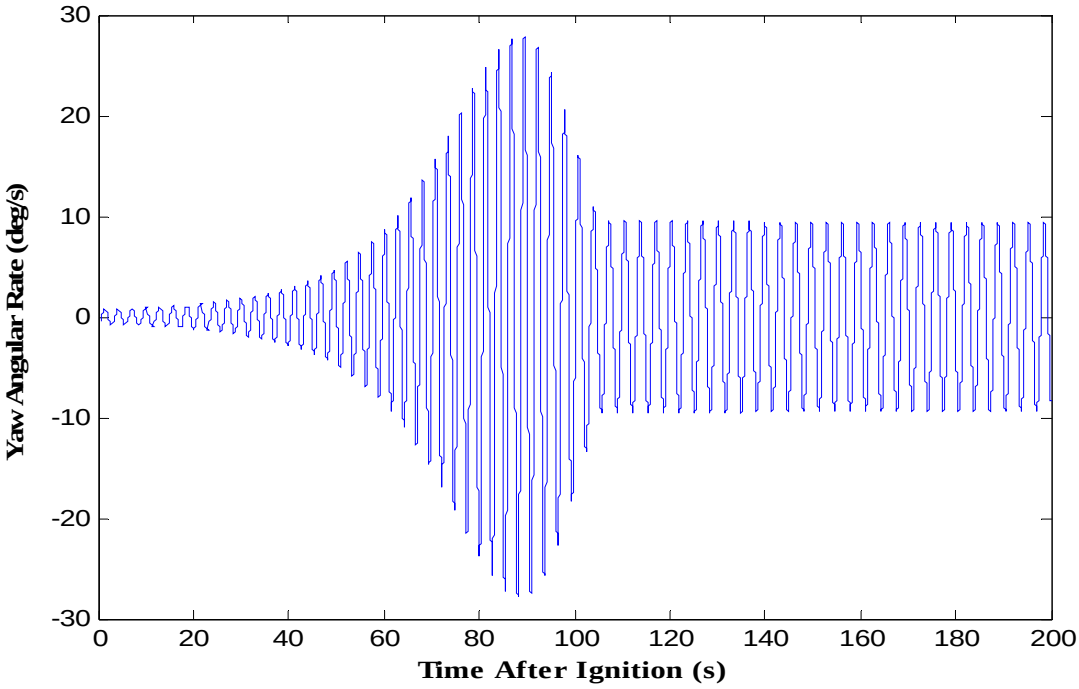

Figure 29 –Yaw Angular Rate vs. Time (Intelsat VI)

The final point in this analysis is the solution to the equation for nutation. The nutation equation's high dependence on the angular rate shows the obvious influence of the angular trend on the change in the coning angle. Figures 30 and 31 show the nutation angle for the Westar and the Intelsat, respectively, throughout burn for an initial tip-off coning angle of 0.1 degrees. The influence in the pattern of growth is quite noticeable for both vehicles. As with the angular rate, the nutation for the Westar continues to grow until burn is ceased. The nutation angle for Intelsat shows the similar observed growth and apparent leveling out as seen in the angular rate figures. As both trends develop, they are contained within an exponential type growth that does not return to the initial coning angle. When burn ceases, they have diverged and remain at whatever angle it is that they achieved taking on the behavior of a rigid body. Figures for the Westar in increments of 0.1 degree tip-off up to one degree can be found in appendix B.

It can be seen in comparison of the figures that the Westar is much more sensitive to initial tip-off than the Intelsat. The most obvious reason for this, it would seem, is that the Intelsat has moments of inertia that are orders of magnitude larger than the Westar. Due to lack of sensitivity to tip-off, appendix B has figures for initial angles of one and five degrees instead of the smaller degree increments.

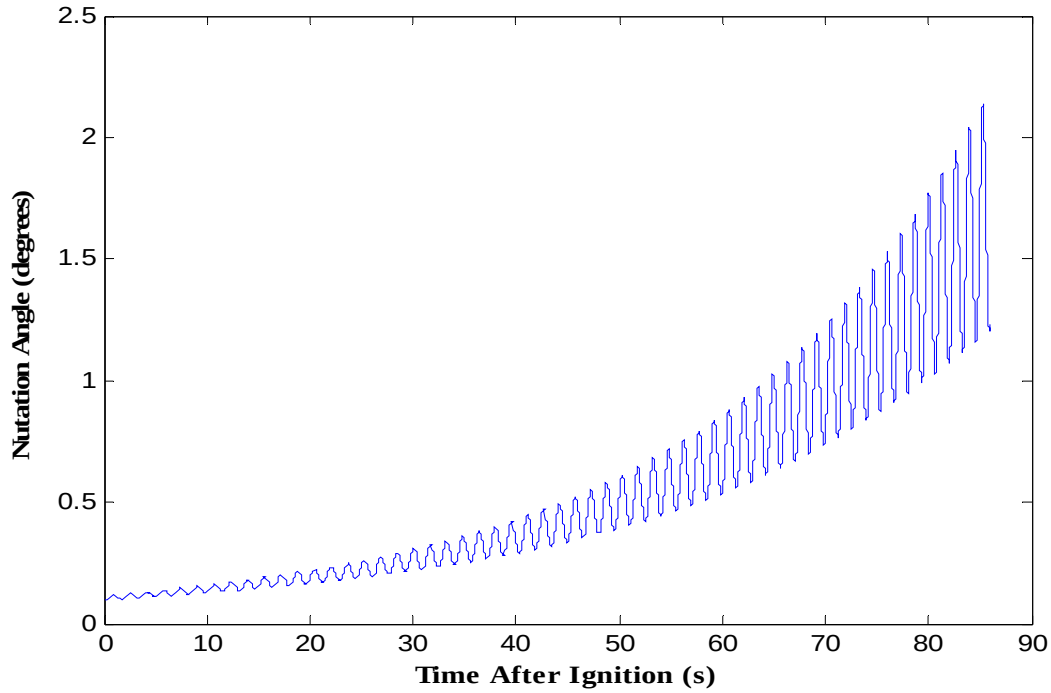

Figure 30– Nutation Angle vs. Time ~ 0.1 Degree Tip-Off (Westar V)

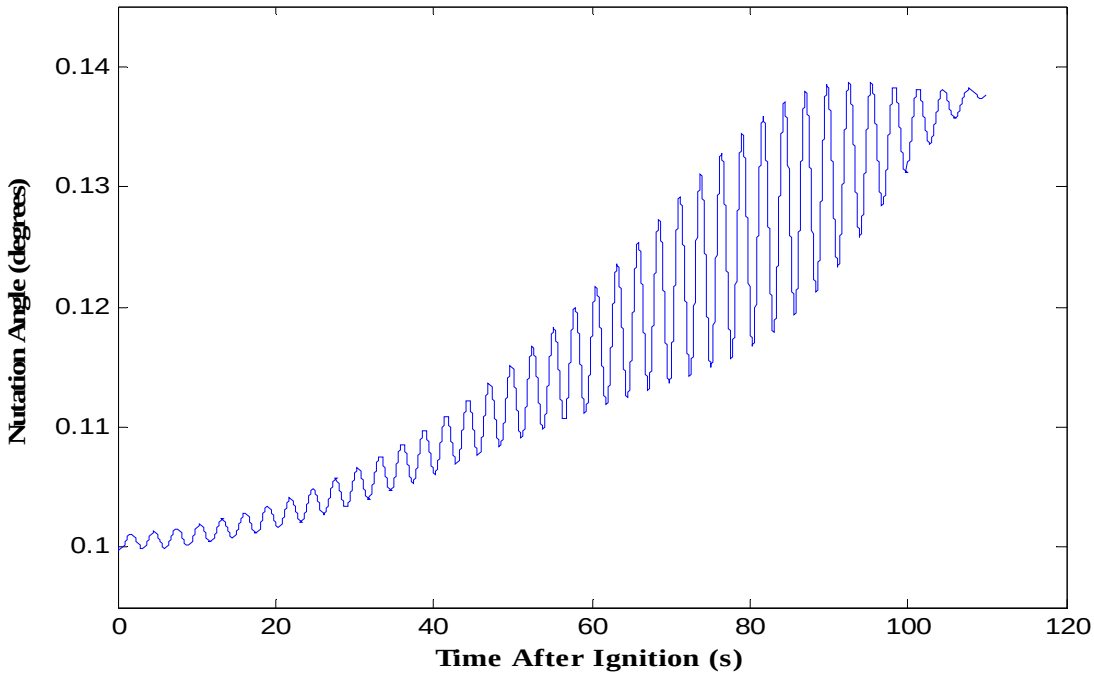

Figure 31– Nutation Angle vs. Time ~ 0.1 Degree Tip-Off (Intelsat VI)

CHAPTER 6

Conclusions

The motivation of this study was to gain an understanding of the effects of energy change on the dynamics of a spinning rocket undergoing loss of mass through a simple manipulation of energy of the system. This was an attempt to understand the nature of the disturbance without a complicated in depth analysis of the gas dynamics of the flow within the combustion chamber. Such previous studies to understand the problem of nutation instability have not yet yielded suitable predictive results or procedures for correction. The current method of correction has been the use of strap-on control devices that cannot properly correct for this unpredictable system behavior. Thus the only way of truly correcting the problem is to understand the exact nature of what is occurring and its dependence on vehicle parameters. Then potential nutation instability can be avoided at the design stage.

It has been found through this study that the jet damping effect, applied from the jet flow as mass is lost, acts as a driving effect in the case of large motors. In the classical explanation of jet damping, the term has been described through its effect on the system moment equations. This analysis has shown that upon rearrangement of these same equations to represent the change in angular rate, it acts as a driving term rather than damping. Therefore, as the angular rates increase their effect on the other terms in the balance of moments overpower any damping effect that this term may exert.

These equations solved for the angular rates, including changing mass effects and jet damping term, showed close similarity to the actual observed angular rate changes in amplitude and growth trend.

A direct dependence of growth on change in mass flow rate can be seen in the graphs of angular rate, increasing for an increase in mass flow rate and decreasing for a decrease. This comes from the driving effect of the jet damping term in the angular rate equations. The computed growth in nutation closely follows the observed growth trends for the angular rates observed in flight data.

The moments of inertia have a more subtle effect on growth. It can be seen that when a vehicle has larger moments of inertia when compared to a vehicle of similar dimensions, it is less susceptible to large disturbances in growth as the limited angular change for the Intelsat shows. The rapidity of the change in moments of inertia due to the large size of the vehicle also encourages a destabilizing growth in vehicles with smaller moments of inertia.

It is suggested that to the results of this analysis can be expanded to aid in design stage of the vehicle. A study of the effects of the dimensions of the vehicle can help designers avoid resulting nutation behavior that may be promoted by increased combustion chamber size. Such calculations remain to be performed in the energy analysis.

The moments of inertia must be altered through changing vehicle size; the mass flow rate can also be modified but that does not lend to an understanding of scale relations. The only way to affect them without changing the mass flow rate is to vary the chamber dimensions. Controlling the shift in center of gravity position relative to the

combustion chamber center of gravity will affect the lateral moment of inertia. This can be altered through use of different propellant grain configurations, such as end burners. Also, the center of gravity position relative to the nozzle exit has an effect on the jet damping term in the angular rate equations. Since it is a squared term and additive, a decrease in this length will decrease effect on the angular rates oscillations.

It was intended to use a simple energy analysis to examine its predictions of nutation instability foregoing complex studies of gas flow. Actual observed oscillations in growth of the angular rates and exponential growth of the nutation angle have been reproduced through its application. It has been demonstrated that the energy method is a useful tool in the study of nutation instability of spinning upper stage vehicles.

REFERENCES

1. Chobotov, Vladimir A. Spacecraft Attitude Dynamics and Control. Krieger Publishing Company, 1991. p. 1, 15-18.

2. Flandro, Gary A., Richard Shorthill, Mark Leloudis, and Robert L. Roach. Flow Induced Nutation Instability in Spinning Solid Propellant Rockets: Final Report. Astronautics Laboratory, August 1989. p. iii-13.

3. Thomson, William Tyrell. Introduction to Space Dynamics. Dover Publications, 1986. p. 5-6, 12, 212-214, 223

4. Wikipedia Encyclopedia. – Nutation. <http://en.wikipedia.org/wiki/Nutation>

5. Flandro, Gary A. Scaling Laws for Propulsion-Induced Nutation Instability of Spin-Stabilized Spacecraft: Final Report. Wasatch Research and Engineering, Inc., 1988-1989. p.2

6. Jet Propulsion-driven Nutational Destabilization of a Spin-stabilized Space Vehicle: Final Report. Hughes Aircraft Company Space and Communication Group. p.2-8, 11, 17

7. Flandro, Gary A. Characteristics of Nutation Instability of Intelsat VI Spin Stabilized Spacecraft during Perigee Propulsion Maneuver: Final Report. Intelsat Organization, August 1988. p. 2, 8-15

8. Boeing Industries. Boeing Integrated Defense Systems/ Satellite Development Center. <http://www.boeing.com/defense-space/space/bss/programs_early.html#early>

APPENDICES

APPENDIX A

Intelsat VI Programs

Call Program for Intelsat VI with Matlab Runge-Kutta Function

```
%%%%%%%%%% Intelsat VI Call Program %%%%%%%%%%
clear;clc;format long;
j=110;
% dt:timestep size
dt=.01;
Tspan=linspace(0,j,j/dt+1);     %%%%%%%%% Linspace Increments Time Span
options = odeset('RelTol',1e-4,'AbsTol',[1e-4,1e-4,1e-4,1e-4]);

%%%%%%%%%% Use of Built-In Runge-Kutta Solver %%%%%%%%%%

%%%%%%%%%% Changing Initial Angle %%%%%%%%%%
%  [t,y] = ode45('initq1intelsatVIomega',Tspan,[-0*pi/180 -.5*pi/180
4.139 .1745/3.25],options);
% [t,y] = ode45('initq1intelsatVIomega',Tspan,[-0*pi/180 -.7*pi/180
5.37 .01745],options);
% [t,y] = ode45('initq1intelsatVIomega',Tspan,[-0*pi/180 -.7*pi/180
5.37 .03488],options);
% [t,y] = ode45('initq1intelsatVIomega',Tspan,[-0*pi/180 -.7*pi/180
5.37 .06978],options);
```

```
% [t,y] = ode45('initq1intelsatVIomega',Tspan,[-0*pi/180 -.7*pi/180
5.37 .08722],options);
% [t,y] = ode45('initq1intelsatVIomega',Tspan,[-0*pi/180 -.7*pi/180
5.37 .10467],options);
% [t,y] = ode45('initq1intelsatVIomega',Tspan,[-0*pi/180 -.7*pi/180
5.37 .12211],options);
% [t,y] = ode45('initq1intelsatVIomega',Tspan,[-0*pi/180 -.7*pi/180
5.37 .13956],options);
% [t,y] = ode45('initq1intelsatVIomega',Tspan,[-0*pi/180 -.7*pi/180 5.37 .157],options);
 [t,y] = ode45('initq1intelsatVIomega',Tspan,[-0*pi/180 -0.3*pi/180
4.139 .01754],options);

%%%%%%%%% Graphing Pitch Angular Rate %%%%%%%%%
figure(1)
plot(t,y(:,1)*180/pi)

%%%%%%%%% Graphing Yaw Angular Rate %%%%%%%%%
figure(2)
plot(t,y(:,2)*180/pi)

%%%%%%%%% Graphing Spin Angular Rate %%%%%%%%%
figure(3)
plot(t,y(:,3))
```

```
%%%%%%%%%% Graphing Nutation Angle %%%%%%%%%%
figure(4)
plot(t,y(:,4)*180/pi)
```

Call Program for Intelsat VI Code with Built Runge-Kutta

```
clear;clc;close all; format long
%initial Conditions
y(1,1)=0;
y(2,1)=-0.7*pi/180;
y(3,1)=5.375;
y(4,1)=.01754;

% p: represents number of cycles
% p=1000;
 dt=.01;
 tmax=200;
% B=11.5;K=0.3;
t=linspace(0,tmax,tmax/dt+1);
for j=1:tmax/dt
    %h = waitbar(0,'Please wait...');
%waitbar(j/(p/dt))
```

```
%close(h)
% Start of Runge Kutta Code
% n : Number of Equations
n=4;
for i=1:4
  for m=1:n
    if (i==1)
       tt=t(j);
         F(m)=y(m,j);
      else
      if (i==4)
         tt=t(j)+dt;
         F(m)=y(m,j)+Dy(m,i-1);
      else
         tt=t(j)+dt/2;
          F(m)=y(m,j)+Dy(m,i-1)/2;
       end
   end
  end
   [Dy]=initRK_1(i,dt,tt,F);
   Dyy(1,i)=Dy(1,i);Dyy(2,i)=Dy(2,i);Dyy(3,i)=Dy(3,i);Dyy(4,i)=Dy(4,i);
end
sum=0;
```

```
 for m=1:n
    sum=sum+1/6*(Dyy(m,1)+2*Dyy(m,2)+2*Dyy(m,3)+Dyy(m,4));
 y(m,j+1)=y(m,j)+sum;
 sum=0;
end
end
%%%%%%%%%% Graphing Pitch Angular Rate %%%%%%%%%%
figure(1)
plot(t,y(1,:)*180/pi)
%%%%%%%%%% Graphing Yaw Angular Rate %%%%%%%%%%
figure(2)
plot(t,y(2,:)*180/pi)
%%%%%%%%%% Graphing Spin Angular Rate %%%%%%%%%%
figure(3)
plot(t,y(3,:))
%%%%%%%%%% Graphing Nutation Angle %%%%%%%%%%
figure(4)
plot(t,y(4,:)*180/pi)
```

Equations Program for Intelsat VI

```
%%%%%%%%%% Equations Program for Intelsat VI %%%%%%%%%%
function dy = initq1intelsatVIomega(t,y);
```

```
dy=zeros(4,1);
I1=16996-2.2986*t-1.5983*t^2+0.0072*t^3;   %% Moments of Inertia (slug-ft^2)
I0=10047+4.1657*t-0.8362*t^2+0.004*t^3;
I1dot=-2.2986-2*1.5983*t+3*0.0072*t^2; %Changes in Moments of Inertia (slug-ft^2/sec)
I0dot=+4.1657-2*0.8362*t+3*0.004*t^2;
Ro=(18.165+0.2827*t-0.0004*t^2)/12;                %%% Chamber Radius (ft)
Lcg=9.3707+0.0007*t+0.0005*t^2-(2E-6)*t^3;         %%% Center of Mass Position (ft)
mdot=-(4.0512+0.0751*t+0.0003*t^2-(2E-5)*t^3);     %%% Mass Flow Rate (slugs/sec)

%%%%%%% Equations Solved to Obtain Three Angular Velocities %%%%%%%
dy(1)=(y(2)*y(3)*(I1-I0)-I1dot*y(1)-mdot*(Lcg)^2*y(1))/I1;
dy(2)=(y(1)*y(3)*(I0-I1)-I1dot*y(2)-mdot*(Lcg)^2*y(2))/I1;
dy(3)=-(I0dot*y(3))/I0;

%%%%%%%%%% Angular Momentum %%%%%%%%%%
 h=I1*(y(1)+y(2))+I0*y(3);

%%%%%%%%%% Rotational Kinetic Energy %%%%%%%%%%
 T=I1*(y(1)^2+y(2)^2)+I0*y(3)^2;
%%%%%%%%%% Angular Momentum Derivative %%%%%%%%%%
hdot=(-mdot*(Lcg^2)*(y(1)+y(2))-y(3)*(I1-I0)*(y(2)-y(1)));
%hdot=I1dot*(y(1)+y(2))+I1*(dy(1)+dy(2))+I0dot*y(3)+I0*dy(3);
%%Using derivative of definition gives same result%%
```

```
%%%%%%%%%% Equation Solved to Obtain Nutation Angle %%%%%%%%%%
 dy(4)=((-(h*hdot*[1-((cos(y(4)))^2)*(1-I1/I0)]/I1)-(((h^2)*((cos(y(4)))^2)*(I0*I1dot-
I1*I0dot))/(2*I1*I0^2))+(T/I1+(y(2)^2+y(1)^2)/2)*I1dot+I1*(y(2)*dy(2)+y(1)*dy(1))+I
0*y(3)*dy(3)+(I0dot*y(3)^2)/2)/(h^2)*cos(y(4))*sin(y(4))*((I0-I1)/I0*I1));
```

Westar V Programs

Call Program for Westar V

```
%%%%%%%%%% Intelsat VI Call Program %%%%%%%%%%
clear;clc;format long;
j=86;
% dt:timestep size
dt=.01;
Tspan=linspace(0,j,j/dt+1);     %%%%%%%%% Linspace Increments Time Span
options = odeset('RelTol',1e-4,'AbsTol',[1e-4,1e-4,1e-4,1e-4]);

%%%%%%%%%% Use of Built-In Runge-Kutta Solver %%%%%%%%%%

%%%%%%%%%% Changing Initial Angle %%%%%%%%%%
%  [t,y] = ode45('initq1omega',Tspan,[-0.3*pi/180 -.5*pi/180 5.37 .1396/3.3],options);
% [t,y] = ode45('initq1omega',Tspan,[-0*pi/180 -0.3*pi/180 5.37 .5],options);
% [t,y] = ode45('initq1omega',Tspan,[-0*pi/180 -.2*pi/180 5.37 .3488],options);
```

```
% [t,y] = ode45('initq1omega',Tspan,[-0*pi/180 -.7*pi/180 5.37 .05233],options);
% [t,y] = ode45('initq1omega',Tspan,[-0*pi/180 -.7*pi/180 5.37 .06978],options);
% [t,y] = ode45('initq1omega',Tspan,[-0*pi/180 -.7*pi/180 5.37 .08722],options);
% [t,y] = ode45('initq1omega',Tspan,[-0*pi/180 -.7*pi/180 5.37 .10467],options);
 [t,y] = ode45('initq1omega',Tspan,[-0*pi/180 -.7*pi/180 5.37 .012211],options);
% [t,y] = ode45('initq1omega',Tspan,[-0*pi/180 -.7*pi/180 5.37 .13956],options);
% [t,y] = ode45('initq1omega',Tspan,[-0*pi/180 -.7*pi/180 5.37 .157],options);
%[t,y] = ode45('initq1omega',Tspan,[-0*pi/180 -.7*pi/180 5.37 .01754],options);


%%%%%%%%% Graphing Pitch Angular Rate %%%%%%%%%
figure(1)
plot(t,y(:,1)*180/pi)
%%%%%%%%% Graphing Yaw Angular Rate %%%%%%%%%
figure(2)
plot(t,y(:,2)*180/pi)
%%%%%%%%% Graphing Spin Angular Rate %%%%%%%%%
figure(3)
plot(t,y(:,3))
 %%%%%%%%% Graphing Nutation Angle %%%%%%%%%
figure(4)
plot(t,y(:,4)*180/pi)
```

Equations Program for Westar V

```
%%%%%%%%%% Equations Program for Westar V %%%%%%%%%%
function dy = initq1omega(t,y);
dy=zeros(4,1);
I1=2124.097-t*(12.932835+0.048777057*t);      %% Moments of Inertia (slug-ft^2)
I0=586.776-t*(0.6186363636+0.027954545454*t);
I1dot=-12.932835-2*0.048777057*t;      %% Changes in Moments of Inertia (slug-ft^2/sec)
I0dot=-0.6186363636-2*0.027954545454*t;
%% Chamber Radius (ft)
Ro=(0.62199872366+t*(0.027987908278+t*(-0.00032505084992+t*(2.6832570372e-6
+t*(5.0587725502e-9-t*3.3371189806e-11)))));
  if Ro>1.90;
    Ro=1.9;
 end
%%%% Center of Mass Position (ft)
Lcg=(6.3025731+t*(0.02190887+t*(-7.55762e-5+t*(2.678833e-6))))/Ro;
 mdot=-(1.349651+0.003086*t);   %%% Mass Flow Rate (slugs/sec)

%%%%%% Equations Solved to Obtain Three Angular Velocities %%%%%%
dy(1)=(y(2)*y(3)*(I1-I0)-I1dot*y(1)-mdot*(Lcg)^2*y(1))/I1;
dy(2)=(y(1)*y(3)*(I0-I1)-I1dot*y(2)-mdot*(Lcg)^2*y(2))/I1;
dy(3)=-(I0dot*y(3))/I0;
```

```
%%%%%%%%%% Angular Momentum %%%%%%%%%%
h=I1*(y(1)+y(2))+I0*y(3);
%%%%%%%%%% Rotational Kinetic Energy %%%%%%%%%%
T=I1*(y(1)^2+y(2)^2)+I0*y(3)^2;
%%%%%%%%%% Angular Momentum Derivative %%%%%%%%%%
hdot=(-mdot*(Lcg^2)*(y(1)+y(2))-y(3)*(I1-I0)*(y(2)-y(1)));
%hdot=I1dot*(y(1)+y(2))+I1*(dy(1)+dy(2))+I0dot*y(3)+I0*dy(3);
%%Using derivative of definition gives same result%%
%%%%%%%%%% Equation Solved to Obtain Nutation Angle %%%%%%%%%%
dy(4)=((-(h*hdot*[1-((cos(y(4)))^2)*(1-I1/I0)]/I1)-(((h^2)*((cos(y(4)))^2)*(I0*I1dot-
I1*I0dot))/(2*I1*I0^2))+(T/I1+(y(2)^2+y(1)^2)/2)*I1dot+I1*(y(2)*dy(2)+y(1)*dy(1))+I
0*y(3)*dy(3)+(I0dot*y(3)^2)/2)/(h^2)*cos(y(4))*sin(y(4))*((I0-I1)/I0*I1));
```

APPENDIX B

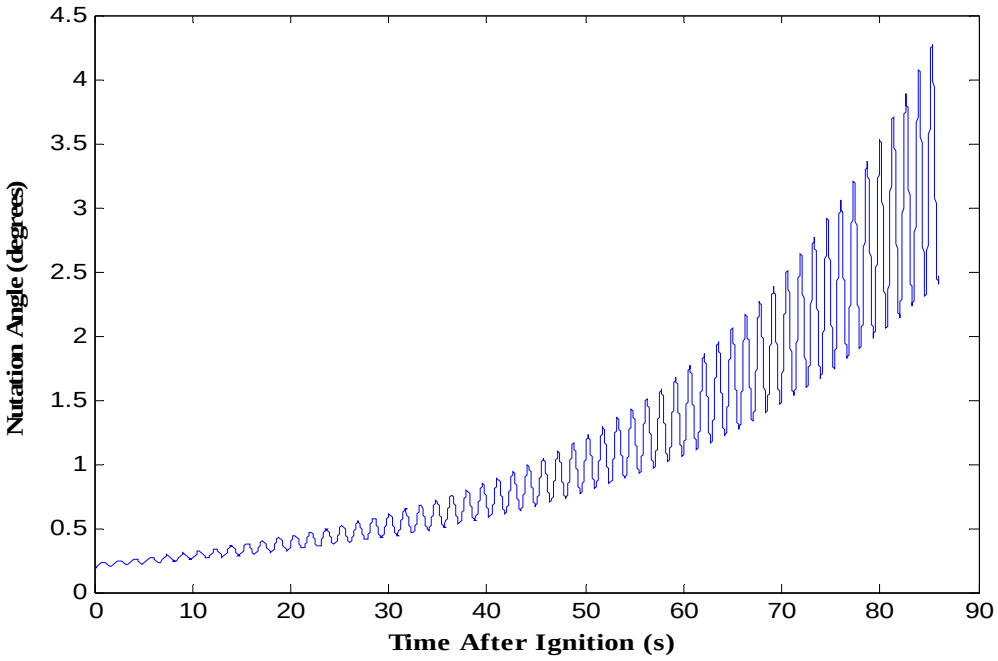

Figure 32 – Nutation Angle vs. Time ~ 0.2 Degree Tip-off (Westar V)

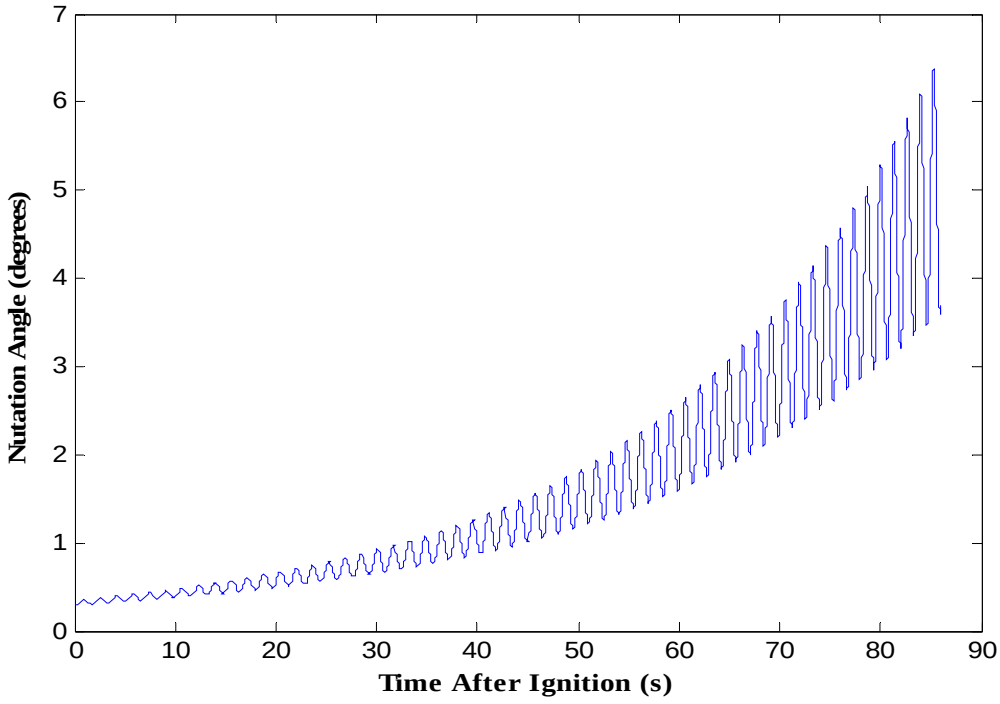

Figure 33 – Nutation Angle vs. Time ~ 0.3 Degree Tip-off (Westar V)

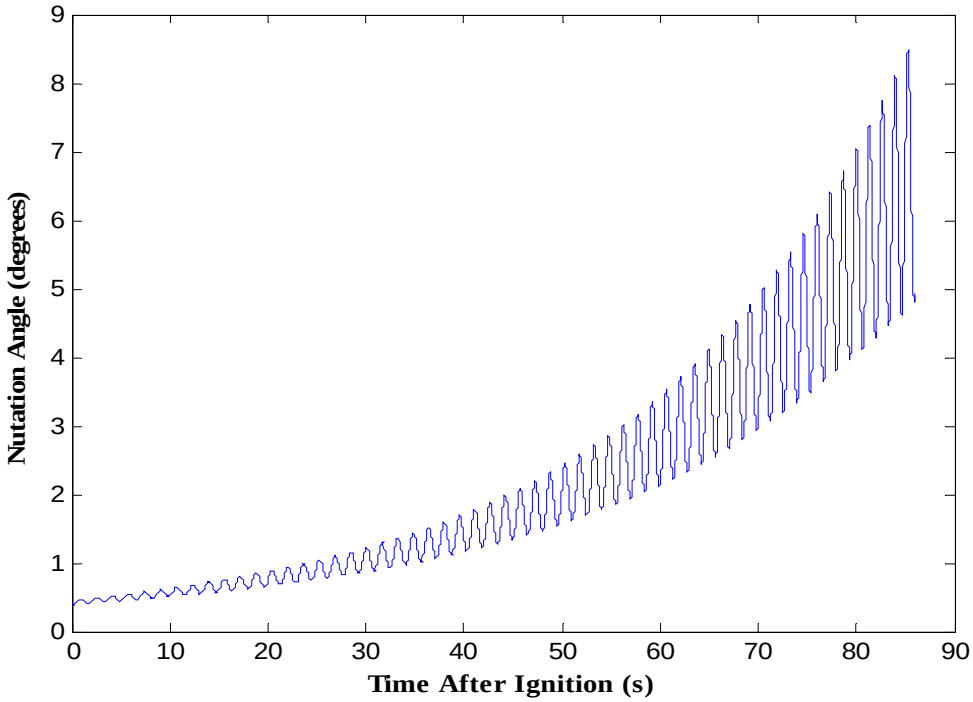

Figure 34 – Nutation Angle vs. Time ~ 0.4 deg Degree Tip-off (Westar V)

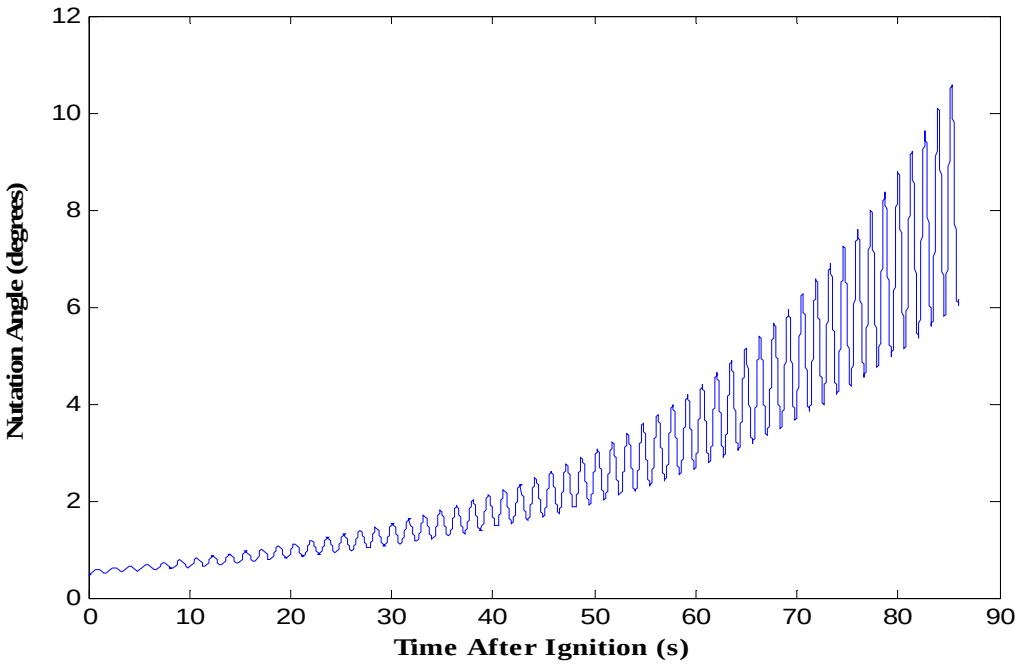

Figure 35 – Nutation Angle vs. Time ~ 0.5 Degree Tip-off (Westar V)

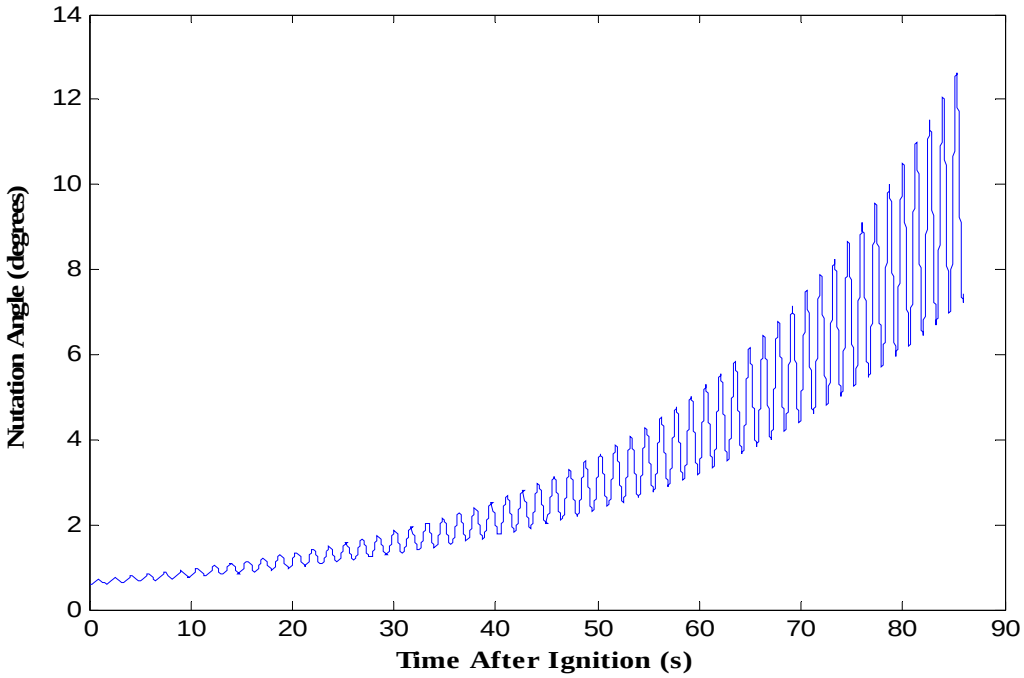

Figure 36 – Nutation Angle vs. Time ~ 0.6 Degree Tip-off (Westar V)

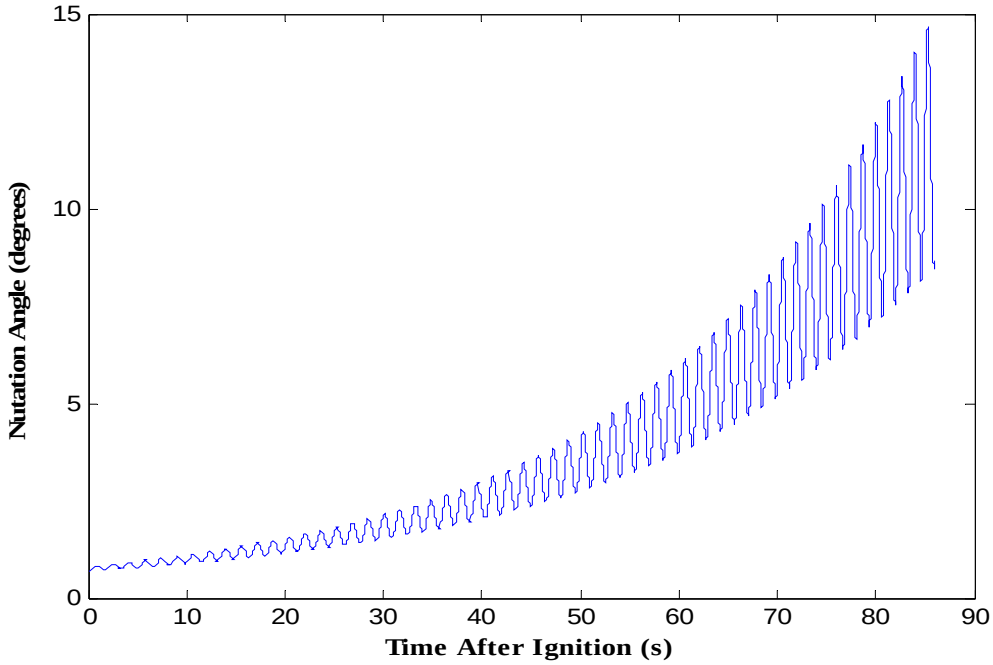

Figure 37 – Nutation Angle vs. Time ~ 0.7 Degree Tip-off (Westar V)

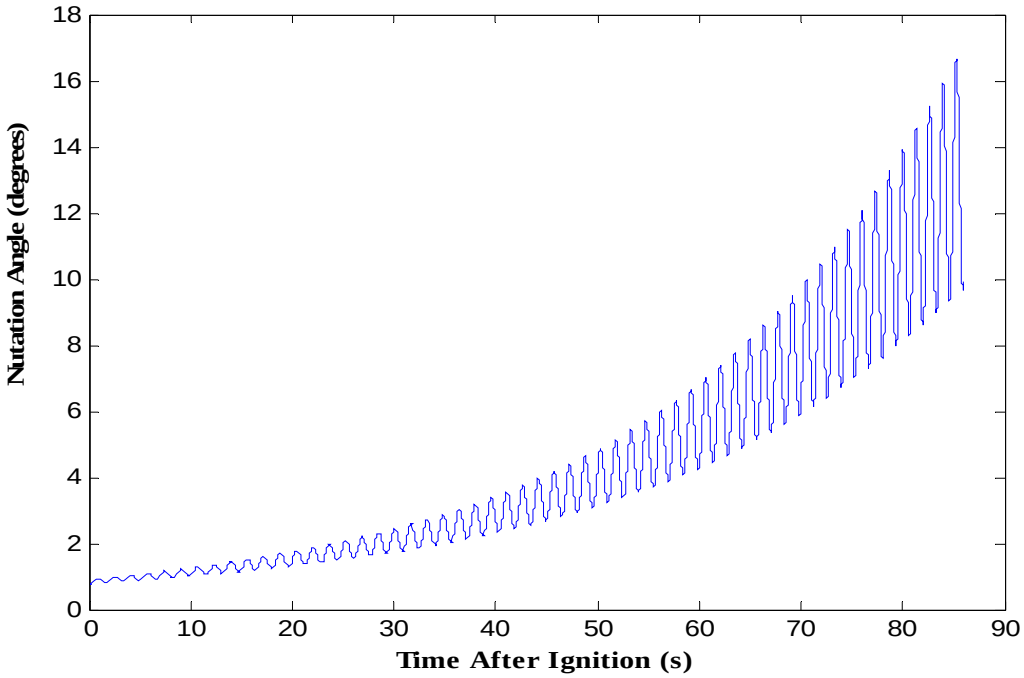

Figure 38 – Nutation Angle vs. Time ~ 0.8 Degree Tip-off (Westar V)

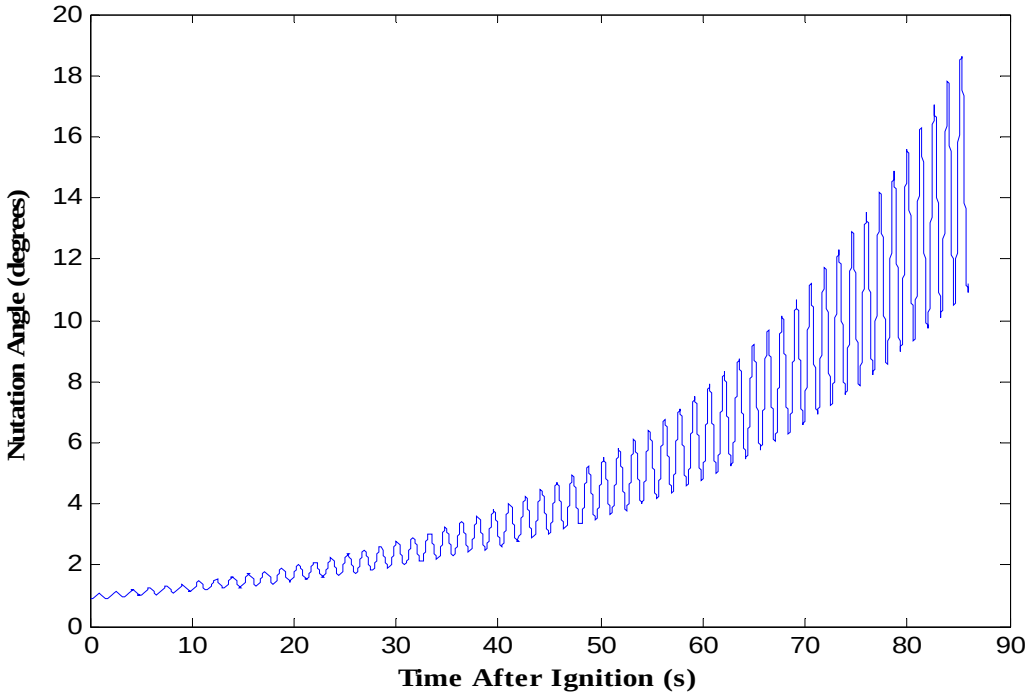

Figure 39 – Nutation Angle vs. Time ~ 0.9 Degree Tip-off (Westar V)

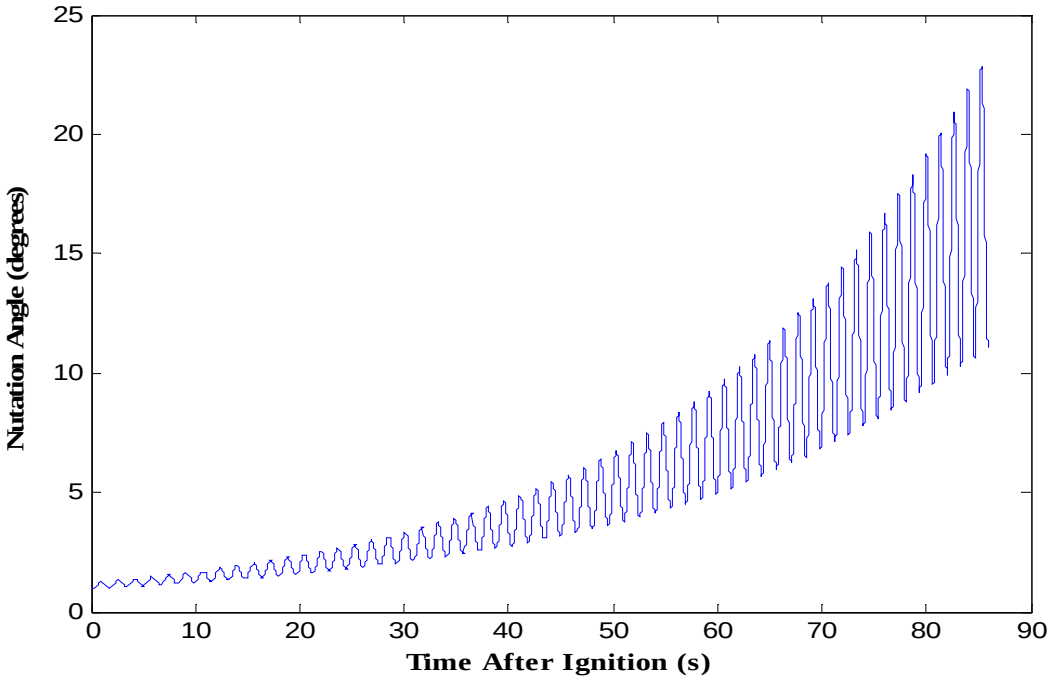

Figure 40 – Nutation Angle vs. Time ~ 1 Degree Tip-off (Westar V)

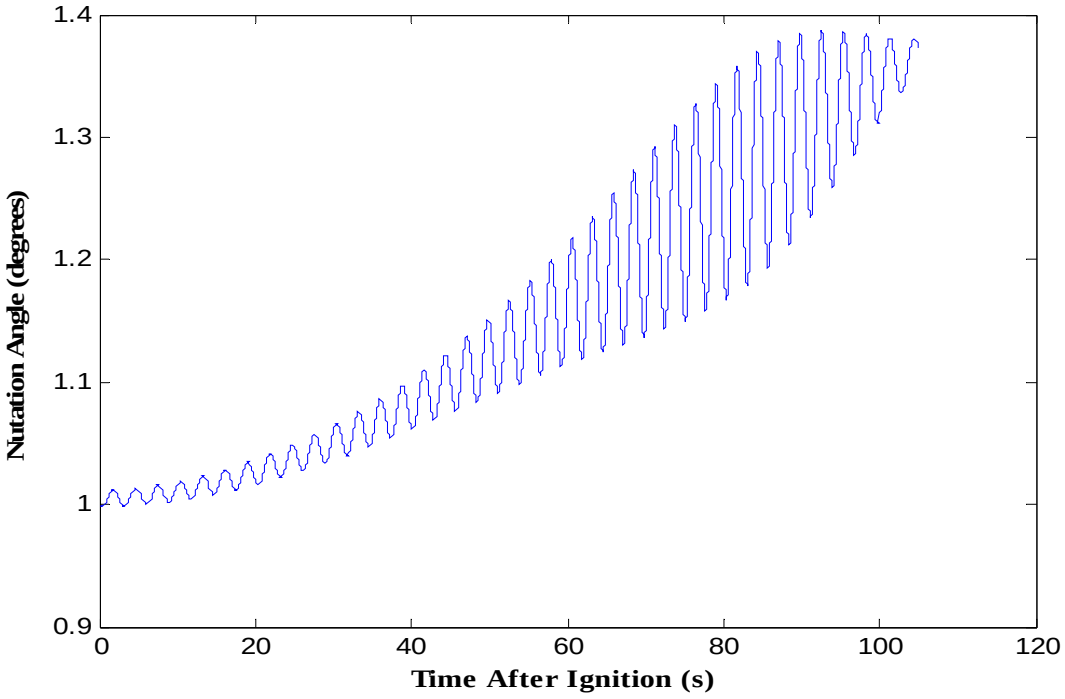

Figure 41– Nutation Angle vs. Time ~ 1 Degree Tip-off (Intelsat VI)

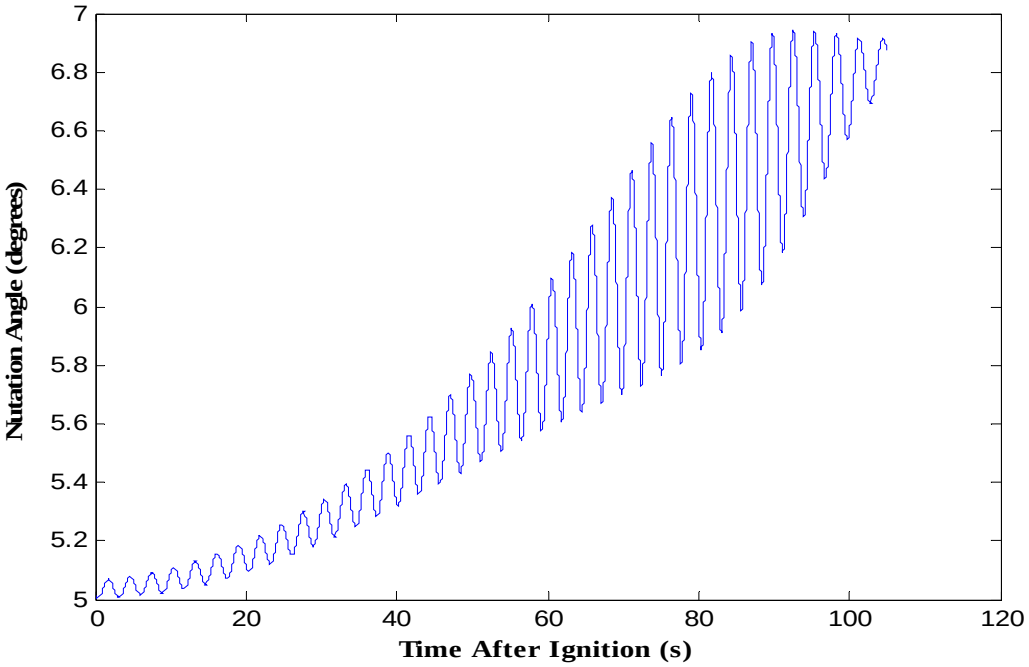

Figure 42– Nutation Angle vs. Time ~ 5 Degree Tip-off (Intelsat VI)

VITA

Tina Morina Rice was born in Dearborn, Michigan in 1982. At the age of four, she and her family moved to Gainesboro, Tennessee to return to where her father was born and raised. Tina graduated from Jackson County High School as Salutatorian in 2000. She attended Tennessee Technological University in Cookeville, Tennessee on a university valedictorian/salutatorian scholarship working in the University Library Archives. While there she took part and leadership in clubs such as ASME, AIAA, and Pi Tau Sigma. She graduated in Spring 2004 with a bachelor's degree in Mechanical Engineering. Tina is now in the Aerospace Engineering Master's degree program at University of Tennessee Space Institute and plans on pursuing a Ph.D. in aerospace engineering as well as another master's degree in aviation systems.